

# 1 Validation of 10-year SAO OMI Ozone Profile (PROFOZ)

## 2 Product Using Ozonesonde Observations

3  
4 Guanyu Huang<sup>1,\*</sup>, Xiong Liu<sup>1</sup>, Kelly Chance<sup>1</sup>, Kai Yang<sup>2</sup>, Pawan K. Bhartia<sup>3</sup>, Zhaonan Cai<sup>1</sup>,  
5 Marc Allaart<sup>4</sup>, Gérard Ancellet<sup>5</sup>, Bertrand Calpini<sup>6</sup>, Gerrie J. R. Coetzee<sup>7</sup>, Emilio Cuevas-  
6 Agulló<sup>8</sup>, Manuel Cupeiro<sup>9</sup>, Hugo De Backer<sup>10</sup>, Manvendra K. Dubey<sup>11</sup>, Henry E. Fuelberg<sup>12</sup>,  
7 Masatomo Fujiwara<sup>13</sup>, Sophie Godin-Beekmann<sup>5</sup>, Tristan J. Hall<sup>12</sup>, Bryan Johnson<sup>14</sup>, Everette  
8 Joseph<sup>15</sup>, Rigel Kivi<sup>16</sup>, Bogumil Kois<sup>17</sup>, Ninong Komala<sup>18</sup>, Gert König-Langlo<sup>19</sup>, Giovanni  
9 Laneve<sup>20</sup>, Thierry Leblanc<sup>22</sup>, Marion Marchand, Kenneth R. Minschwaner<sup>23</sup>, Gary Morris<sup>24</sup>,  
10 Michael J. Newchurch<sup>25</sup>, Shin-Ya Ogino<sup>26</sup>, Nozomu Ohkawara<sup>27</sup>, Ankie J. M. PETERS<sup>4</sup>, Françoise  
11 Posny<sup>28</sup>, Richard Querel<sup>29</sup>, Rinus Scheele<sup>4</sup>, Frank J. Schmidlin<sup>3</sup>, Russell C. Schnell<sup>14</sup>, Otto  
12 Schrems<sup>19</sup>, Henry Selkirk<sup>30</sup>, Masato Shiotani<sup>31</sup>, Pavla Skrivánková<sup>32</sup>, René Stübi<sup>6</sup>, Ghassan  
13 Taha<sup>30</sup>, David W. Tarasick<sup>33</sup>, Anne M. Thompson<sup>3</sup>, Valérie Thouret<sup>34</sup>, Matt Tully<sup>35</sup>, Roeland  
14 van Malderen<sup>10</sup>, , Holger Vömel<sup>36</sup>, Peter von der Gathen<sup>37</sup>, Jacquelyn C. Witte<sup>38</sup>, Margarita  
15 Yela<sup>39</sup>

- 16 1. Harvard-Smithsonian Center for Astrophysics, Cambridge, MA, USA
- 17 2. Department of Atmospheric and Oceanic Science, University of Maryland, College Park,  
18 Maryland, USA
- 19 3. NASA Goddard Space Flight Center, Greenbelt, Maryland, USA
- 20 4. Royal Netherlands Meteorological Institute (KNMI), De Bilt, the Netherlands
- 21 5. LATMOS-ISPL, Université Paris 6 Pierre-et-Marie-Curie, Paris, France
- 22 6. MeteoSwiss Aerological Station, Federal Office of Meteorology and Climatology  
23 MeteoSwiss, Payerne, Switzerland
- 24 7. South African Weather Service, Pretoria, South Africa
- 25 8. Izana Atmospheric Research Center, Meteorological State Agency of Spain, Santa Cruz de  
26 Tenerife, Spain
- 27 9. National Meteorological Service, Ushuaia, Tierra del Fuego, Argentina
- 28 10. Royal Meteorological Institute of Belgium, Brussel, Belgium
- 29 11. Los Alamos National Laboratory, Los Alamos, NM, USA

- 30 12. Earth, Ocean and Atmospheric Sciences, Florida State University, Tallahassee, FL, USA
- 31 13. Faculty of Environmental Earth Science, Hokkaido University, Sapporo, Japan
- 32 14. NOAA/ESRL Global Monitoring Division, Boulder, CO, USA
- 33 15. Atmospheric Sciences Research Center, SUNY University at Albany, Albany, NY, USA
- 34 16. Finnish Meteorological Institute, Helsinki, Finland
- 35 17. The Institute of Meteorology and Water Management, National Research Institute, Warsaw,
- 36 Poland
- 37 18. Indonesian Institute of Aeronautics and Space (LAPAN), Bandung, Indonesia
- 38 19. Alfred Wegener Institute for Polar and Marine Research, Bremerhaven, Germany
- 39 20. Earth Observation Satellite Images Applications Lab (EOSIAL), Università di Roma 'La
- 40 Sapienza', Rome, Italy
- 41 21. Danish Meteorological Institute, Copenhagen, Denmark
- 42 22. Jet Propulsion Laboratory, California Institute of Technology, Pasadena, CA, USA
- 43 23. Department of Physics, New Mexico Institute of Mining and Technology, Socorro, NM,
- 44 USA
- 45 24. St. Edward's University, Austin, TX, USA
- 46 25. Department of Atmospheric Science, University of Alabama in Huntsville, Huntsville, AL,
- 47 USA
- 48 26. Department of Coupled Ocean-Atmosphere-Land Processes Research, Japan Agency for
- 49 Marine-Earth Science and Technology, Yokosuka, Japan
- 50 27. Global Environment and Marine Department, Japan Meteorological Agency, Tokyo, Japan
- 51 28. Université de la Réunion, Saint Denis, France
- 52 29. National Institute of Water and Atmospheric Research, Lauder, Central Otago, New Zealand
- 53 30. Universities Space Research Association, Greenbelt, MD, USA
- 54 31. Research Institute for Sustainable Humanosphere, Kyoto University, Kyoto, Japan
- 55 32. Upper Air and Surface Observation Department, Czech Hydrometeorological Institute,
- 56 Praha, Czech Republic
- 57 33. Air Quality Research Division, Environment & Climate Change Canada, Downsview, ON,
- 58 Canada.
- 59 34. Laboratoire d'Aerologie, Université de Toulouse, Toulouse, France

- 60 35. Observations & Infrastructure Division, Bureau of Meteorology, Melbourne, Victoria,  
61 Australia
- 62 36. Earth Observing Laboratory, National Center for Atmospheric Research, Boulder, CO, USA
- 63 37. Alfred Wegener Institute, Potsdam, Germany
- 64 38. Science Systems and Applications Inc. Greenbelt, MD, USA
- 65 39. Atmospheric Research and Instrumentation Branch, National Institute for Aerospace  
66 Technology (INTA), Madrid, Spain
- 67 \*Correspondence to: Guanyu Huang ([guanyu.huang@cfa.harvard.edu](mailto:guanyu.huang@cfa.harvard.edu))

68 **Abstract**

69 We validate the Ozone Monitoring Instrument (OMI) ozone-profile (PROFOZ) product from  
70 October 2004 through December 2014 retrieved by the Smithsonian Astrophysical Observatory  
71 (SAO) algorithm against ozonesonde observations. We also evaluate the effects of OMI Row  
72 anomaly (RA) on the retrieval by dividing the data set into before and after the occurrence of  
73 serious OMI RA, i.e., pre-RA (2004-2008) and post-RA (2009-2014). The retrieval shows good  
74 agreement with ozonesondes in the tropics and mid-latitudes and for pressure  $< \sim 50$  hPa in the  
75 high latitudes. It demonstrates clear improvement over the a priori down to the lower troposphere  
76 in the tropics and down to an average of  $\sim 550$  (300) hPa at middle (high latitudes). In the tropics  
77 and mid-latitudes, the profile mean biases (MBs) are less than 6%, and the standard deviations  
78 (SDs) range from 5-10% for pressure  $< \sim 50$  hPa to less than 18% (27%) in the tropics (mid-  
79 latitudes) for pressure  $> \sim 50$  hPa after applying OMI averaging kernels to ozonesonde data. The  
80 MBs of the stratospheric ozone column (SOC, the ozone column from the tropopause pressure to  
81 the ozonesonde burst pressure) are within 2% with SDs of  $< 5\%$  and the MBs of the tropospheric  
82 ozone column (TOC) are within 6% with SDs of 15%. In the high latitudes, the profile MBs are  
83 within 10% with SDs of 5-15% for pressure  $< \sim 50$  hPa, but increase to 30% with SDs as great as  
84 40% for pressure  $> \sim 50$  hPa. The SOC MBs increase up to 3% with SDs as great as 6% and the  
85 TOC SDs increase up to 30%. The comparison generally degrades at larger solar-zenith angles  
86 (SZA) due to weaker signals and additional sources of error, leading to worse performance at  
87 high latitudes and during the mid-latitude winter. Agreement also degrades with increasing  
88 cloudiness for pressure  $> \sim 100$  hPa and varies with cross-track position, especially with large  
89 MBs and SDs at extreme off-nadir positions. In the tropics and mid-latitudes, the post-RA  
90 comparison is considerably worse with larger SDs reaching 2% in the stratosphere and 8% in the  
91 troposphere and up to 6% in TOC. There are systematic differences that vary with latitude  
92 compared to the pre-RA comparison. The retrieval comparison demonstrates good long-term  
93 stability during the pre-RA period, but exhibits a statistically significant trend of 0.14-0.7%/year  
94 for pressure  $< \sim 80$  hPa, 0.7 DU/year in SOC and -0.33 DU/year in TOC during the post-RA  
95 period. The spatiotemporal variation of retrieval performance suggests the need to improve  
96 OMI's radiometric calibration especially during the post-RA period to maintain the long-term  
97 stability and reduce the latitude/season/SZA and cross-track dependence of retrieval quality.

## 98 **1 Introduction**

99 The Dutch-Finnish built Ozone Monitoring Instrument (OMI) on board the NASA Aura satellite  
100 has been making useful measurements of trace gases including ozone and aerosols since October  
101 2004. There are various retrieval algorithms to retrieve ozone profile and/or total ozone from  
102 OMI data (Bak et al., 2015), including two independent operational total ozone algorithms  
103 (Bhartia and Wellemeyer, 2002; Veefkind et al., 2006) and two ozone profile algorithms. Of the  
104 two ozone profile algorithms, one is the operational algorithm (OMO3PR) developed at KNMI  
105 (van Oss et al., 2001), and the other one is a research algorithm developed at Smithsonian  
106 Astrophysical Observatory (SAO) by (Liu et al., 2010b). Both algorithms retrieve ozone profile  
107 from the spectral region 270-330 nm using the optimal estimation method, but they differ  
108 significantly in implementation details including radiometric calibration, radiative transfer model  
109 simulation, a priori constraint, retrieval grids, and additional retrieval parameters. The SAO  
110 ozone profile retrieval algorithm was initially developed for Global Ozone Monitoring  
111 Experiment (GOME) data and was adapted to OMI data (Liu et al., 2010b). Total ozone column  
112 (OC), Stratospheric Ozone Column (SOC) and Tropospheric Ozone Column (TOC) can be  
113 directly derived from the retrieved ozone profile with retrieval errors in the range of a few  
114 Dobson Units (DU) (Liu et al., 2006b; Liu et al., 2010a). This algorithm has been put into  
115 production in the OMI Science Investigator-led Processing System (SIPS), processing the entire  
116 OMI data record with approximately one-month delay. The ozone profile product titled  
117 PROFOZ is publicly available at the Aura Validation Data Center (AVDC)  
118 (<http://avdc.gsfc.nasa.gov/index.php?site=2045907950>). This long-term ozone profile product,  
119 with high spatial resolution and daily global coverage, constitutes a useful dataset to study the  
120 spatial and temporal distribution of ozone.

121 To effectively use the retrieval dataset, it is necessary to evaluate and understand its retrieval  
122 quality and long-term performance. Although validation of the ozone profile product (mostly  
123 earlier versions) has been partially performed against aircraft, ozonesonde, and Microwave Limb  
124 Sounder (MLS) data, these evaluations are limited to certain time periods and/or spatial region  
125 and/or to only portion of the product (e.g., total ozone columns (OC) or TOC only) (Bak et al.,  
126 2013a; Hayashida et al., 2015; Lal et al., 2013; Liu et al., 2010a; Liu et al., 2010b; Pittman et al.,  
127 2009; Sellitto et al., 2011; Wang et al., 2011; Yang et al., 2007; Ziemke et al., 2014).

128 Additionally, the quality of ozone profile retrievals is very sensitive to the signal to noise ratio  
129 (SNR) of the radiance measurements as well as their radiometric calibration, which may degrade  
130 over time as shown in GOME and GOME-2 retrievals (Cai et al., 2012; Liu et al., 2007).  
131 Although OMI's optical degradation is remarkably small to within 1-2% over the years, the SNR  
132 and the number of good spectral pixels (not flagged as bad/hot pixels) have been gradually  
133 decreasing over the years due to the expected CCD degradation (Claas, 2014). Furthermore, the  
134 occurrence of RA, which affects level 1b data at all wavelengths for particular viewing directions  
135 or cross-track positions and likely due to blocking objects in the optical path, started in June  
136 2007 affecting a few positions. This effect abruptly worsened in January 2009 affecting ~1/3 of  
137 the cross-track positions (Kroon et al., 2011). The impacts of RA not only evolve with time but  
138 also vary over the duration of an orbit. Analysis indicates that radiances in the UV1 channels  
139 (shorter than ~310 nm) used in our retrievals might have been affected at all positions (Personal  
140 communication with S. Marchenko) and are not adequately flagged for RA. Therefore, we need  
141 to evaluate the impacts of instrument degradation and especially row anomaly on the temporal  
142 performance of our ozone profile product. Currently, we are planning an update of the ozone  
143 profile algorithm to maintain the long-term consistency of the product. The update will include  
144 empirical correction of systematic errors caused by the instrument degradation and row anomaly  
145 as a function of time. Such correction also requires us to evaluate the long-term retrieval quality  
146 of our product.

147 To understand retrieval quality and the resulting spatial and temporal performance of our OMI  
148 product, we evaluate our data from October 2004 through December 2014 against available  
149 ozonesonde and MLS observations, respectively, in two papers. This paper evaluates our ozone  
150 product including both ozone profiles and stratospheric and tropospheric ozone columns using  
151 ozonesonde observations with a focus on retrieval quality in the troposphere. More than 27,000  
152 ozonesonde profiles from both regular ozonesonde stations and field campaigns are used in this  
153 study to provide a comprehensive and global assessment of the long-term quality of our OMI  
154 ozone product. This paper is followed by the validation against collocated MLS data with a focus  
155 on the retrieval quality in the stratosphere (Huang et al., 2017), also submitted to this special  
156 issue).

157 This paper is organized as follows: Section 2 describes OMI retrievals and ozonesonde data. The  
158 validation methodology is introduced in Section 3. Section 4 presents results, analysis and  
159 discussions regarding the OMI and ozonesonde comparisons. Section 5 summarizes and  
160 concludes this study.

## 161 **2 OMI and Ozonesonde Datasets**

### 162 **2.1 OMI and OMI Ozone Profile Retrievals**

163 OMI is a Dutch-Finnish built nadir-viewing pushbroom UV/visible instrument aboard the NASA  
164 Earth Observing System (EOS) Aura satellite that was launched into a sun-synchronous orbit in  
165 July 2004. It measures backscattered radiances in three channels covering the 270-500 nm  
166 wavelength range (UV1: 270-310 nm, UV2: 310-365 nm, visible: 350-500 nm) at spectral  
167 resolutions of 0.42-0.63 nm (Levelt et al., 2006). Measurements across the track are binned to  
168 60 positions for UV2 and visible channels, 30 positions for the UV1 channels due to the weaker  
169 signals. This results in daily global coverage with a nadir spatial resolution of 13 km  $\times$  24 km  
170 (along  $\times$  across track) for UV2 and visible channels, and 13 km  $\times$  48 km for the UV1 channel.

171 The SAO OMI ozone profile algorithm was adapted from the GOME ozone profile algorithm  
172 (Liu et al., 2005) to OMI and was initially described in detail in Liu et al. (2010b). Profiles of  
173 partial ozone columns are retrieved at 24 layers,  $\sim$ 2.5 km for each layer, from the surface to  $\sim$ 60  
174 km using OMI radiance spectra in the spectral region 270-330 nm with the optimal estimation  
175 technique. In addition to the OC, SOC and TOC can be directly derived from the retrieved ozone  
176 profile with the use of tropopause (defined based on the lapse rate) from the daily National  
177 Center for Environmental Protection (NCEP) reanalysis data. The retrievals are constrained with  
178 month- and latitude-dependent climatological a priori profiles derived from 15-year ozonesonde  
179 and SAGE/MLS data (McPeters et al., 2007) with considerations of OMI random-noise errors.  
180 OMI radiances are pre-calibrated based on two days of average radiance differences in the  
181 tropics between OMI observations and simulations with zonal mean MLS data for pressure less  
182 than 215 hPa and climatological ozone profile for pressure greater than 215 hPa. This “soft  
183 calibration” varies with wavelength and cross-track positions but does not depend on space and  
184 time.

185 The current algorithm of our SAO OMI ozone product that is used in this paper was briefly  
186 described in Kim et al. (2013). The radiative transfer calculations have been improved through  
187 the convolution of simulated radiance spectra at high resolutions rather than effective cross  
188 sections, which is done by interpolation from calculation at selected wavelengths assisted by  
189 weighting function. In addition, four spatial pixels along the track are coadded to speed up  
190 production processes at a nadir spatial resolution of 52 km × 48 km. Meanwhile, minimum  
191 measurement errors of 0.4% and 0.2% are imposed in the spectral ranges 270-300 nm and 300-  
192 330 nm, respectively, to stabilize the retrievals. The use of floor errors typically reduces the  
193 Degree of Freedom for Signals (DFS) and increases retrieval errors. Compared to the initial  
194 retrievals, the average total, stratospheric, and tropospheric DFS decrease by 0.49, 0.27, and  
195 0.22, respectively, and the mean retrieval errors in OC, SOC, and TOC increase by 0.6, 0.5, and  
196 1.2 DU, respectively. The corresponding changes to the retrievals are generally within retrieval  
197 uncertainties except for a systematic increase in tropospheric ozone at SZA larger than ~75°,  
198 where the TOC increases to ~12 DU. Validation against ozonesonde data indicates that this TOC  
199 increase at large SZA makes the retrieval worse. Therefore retrieved tropospheric ozone at such  
200 large SZA should not be used, but the retrieved total ozone still shows good quality (Bak et al.,  
201 2015).

202 For current products, retrievals contain ~5.5-7.4 DFS, with 4.6-7.3 in the stratosphere and 0-1.2  
203 in the troposphere. Vertical resolution varies generally from 7–11 km in the stratosphere to 10–  
204 14 km in the troposphere, when there is adequate retrieval sensitivity to the tropospheric ozone.  
205 Retrieval random-noise errors (i.e., precisions) typically range from 0.6–2.5 % in the middle  
206 stratosphere to approximately 12% in the lower stratosphere and troposphere. The solution  
207 errors, dominated by smoothing errors, vary generally from 1-7% in the middle stratosphere to 7-  
208 38% in the troposphere. The solution errors in the integrated OC, SOC, and TOC are typically in  
209 the few DU range. Errors caused by the forward model and forward model parameter  
210 assumptions are generally much smaller than the smoothing error (Liu et al., 2005). The main  
211 sources of these errors include systematic errors in temperature and cloud-top pressure.  
212 Systematic measurement errors are the most difficult to estimate, mostly due to lack of full  
213 understanding of the OMI instrument calibration.



214 Certain cross track positions in OMI data have been affected by RA since June 2007 (Kroon et  
215 al., 2011). Loose thermal insulating material in front of the instrument's entrance slit is believed  
216 to block and scatter light, causing measurement error. The anomaly affects radiance  
217 measurements at all wavelengths for specific cross-track viewing directions that are imaged to  
218 CCD rows. Initially, the anomaly only affected a few rows. But since January 2009, the anomaly  
219 has spread to other rows and shifted with time. The RA also shows slight differences among  
220 different spectral channels, and varies during the duration of an orbit. Pixels affected by the RA  
221 are flagged in the level 1b data. The science team suggested that they are not be used in research.  
222 For data before 2009, the RA flagging is not applied in the processing. Pixels seriously affected  
223 by RA will typically show enhanced fitting residuals. The algorithm was updated to use RA  
224 flagging in the UV1 channel and was used to process the data starting from 2009. If a pixel is  
225 flagged as a row anomaly then it is subsequently not retrieved to speed up the processing except  
226 that the cross-track position 24 is still retrieved due to reasonably good fitting. It should be noted  
227 that the retrieval quality of those non-flagged pixels may still be affected by the RA, because of  
228 the different RA flagging in the UV1 and UV2, the lack of RA flagging before 2009 and  
229 inadequacy of the RA flagging.

230 To screen out OMI profiles for validation, we only use OMI ozone profiles meeting the  
231 following criteria based on three filtering parameters: 1) nearly clear-sky scenes with effective  
232 cloud fraction less than 0.3; 2) cross track positions between 4 and 27, due to the relatively worse  
233 quality and much larger footprint size of the off-nadir pixels beyond this range; 3) SZA should  
234 be less than  $75^\circ$  due to very limited retrieval sensitivity to tropospheric ozone and the  
235 aforementioned positive biases. The selection and justification of these criteria will be discussed  
236 in Sects. 2.1.2-4.1.4, in which we will use all OMI pixels of each filtering parameter when  
237 evaluating retrieval quality as a function of that specific parameter. The fitting quality of each  
238 retrieval is shown in the fitting RMS (root mean square of the fitting residuals relative to the  
239 assumed measurement errors). The mean fitting RMS including both UV1 and UV2 channels has  
240 been increasing with time as shown in Figure 1. This is primarily due to the increase of fitting  
241 residuals in UV1 caused by the instrument degradation and RA since the fitting residuals of UV2  
242 only slightly increase with time. As aforementioned, the retrieval information of stratospheric  
243 and tropospheric ozone mainly comes from UV1 and UV2, respectively. Consequently, retrievals

244 in the troposphere, the focus of this paper, are less impacted by the increasing fitting RMS.  
245 However, to apply consistent filtering in validation against both ozonesonde in this study and  
246 MLS data in the companion paper (Huang et al., 2017), we set the RMS threshold based on the  
247 overall fitting RMS and select retrievals with fitting RMS smaller than the sum of monthly mean  
248 RMS and its  $2\sigma$  (i.e., Standard Deviations (SDs) of fitting RMS).

## 249 **2.2 Ozonesondes**

250 The balloon-borne ozonesonde is a well-established technique to observe the ozone profile from  
251 the surface to  $\sim 35$  km with vertical resolution of  $\sim 100$ - $150$  m and approximately 3-5% precision  
252 and 5-10% accuracy (Deshler et al., 2008; Johnson, 2002; Komhyr, 1986; Komhyr et al., 1995;  
253 Smit et al., 2007). Ozonesonde data have been widely used in the studies of stratospheric ozone,  
254 climate change, tropospheric ozone and air quality, as well as the validation of satellite  
255 observations (Huang et al., 2015; Kivi et al., 2007; Thompson et al., 2015; Wang et al., 2011).  
256 However, the accuracy of ozonesonde observations depends on data processing technique, sensor  
257 solution, and instrument type and other factors. Consequently, station-to-station biases may  
258 occur in ozonesonde measurements and could be as great as 10% (Thompson et al., 2007c;  
259 Worden et al., 2007).

260 A decade (2004-2014) of global ozonesonde data with locations shown in Figure 2, are utilized  
261 in this study to validate our OMI ozone profile product. Most of our ozonesonde data were  
262 obtained from the Aura Validation Data Center (AVDC) archive. It contains routine launches  
263 from ozonesonde stations, mostly weekly and occasionally 2-3 times a week at some stations. It  
264 also collects launches from field campaigns, for instance, IONS 06 (INTEX-B Ozone Network  
265 Study 2006), ARCIONS (Arctic Intensive Ozonesonde Network Study)  
266 (<http://croc.gsfc.nasa.gov/arcions/>) (Tarasick et al., 2010; Thompson et al., 2008). Data not  
267 available at AVDC are obtained from other archives such as the World Ozone and Ultraviolet  
268 Radiation Data Center (WOUDC) (<http://woudc.org/>), the Southern Hemisphere Additional  
269 Ozonesondes (SHADOZ) (Thompson et al., 2007a; Thompson et al., 2007b), as well as archives  
270 of recent field campaigns including DISCOVER-AQ (Deriving Information on Surface  
271 Conditions from Column and Vertically Resolved Observations Relevant to Air Quality,  
272 <http://discover-aq.larc.nasa.gov/>) (Thompson et al., 2015) and SEACR<sup>4</sup>S (Studies of Emissions

273 and Atmospheric Composition, Clouds and Climate Coupling by Regional Surveys,  
274 <https://espo.nasa.gov/home/seac4rs>) (Toon et al., 2016). Almost all of the ozonesonde data in  
275 this study were obtained from electrochemical concentration cell (ECC) ozonesondes, which is  
276 based on the oxidation reaction of ozone with potassium iodide (KI) in solution. The exceptions  
277 are Hohenpeissenberg station in Germany that uses Brewer-Mast (BM) ozonesondes, the New  
278 Delhi, Poona, and Trivandrum stations that use Indian ozonesondes, and four Japanese stations  
279 (i.e., Sapporo, Tsukuba, Naha and Syowa) that switched from KC ozonesondes to ECC  
280 ozonesondes during late 2008 and early 2010. These types of ozonesondes have been reported to  
281 have larger uncertainties than ECC ozonesondes (Hassler et al., 2014; Liu et al., 2013; WMO,  
282 1998).

283 To avoid using anomalous profiles, we screen out ozonesondes that burst at pressure exceeding  
284 200 hPa, ozone profiles with gaps greater than 3 km, more than 80 DU TOC or less than 100 DU  
285 SOC. In the SOC comparison, we also filter measurements that do not reach 12 hPa. Some  
286 ozonesonde data used in this paper (e.g. WOUDC data) are provided with a correction factor  
287 (CF) derived by normalizing the integrated ozone column (appended with ozone climatology  
288 above burst altitude) to the coincident total ozone column measured by a Dobson or Brewer  
289 instrument to account for uncertainties mainly from the pump efficiency especially near the top  
290 of the profiles. The CF is also included in our screening processes. If the CF is available, we  
291 select ozonesonde profiles with the CF in the range of 0.85 to 1.15 to filter profiles that require  
292 too much correction, and apply the correction. Finally, a small number of obviously erroneous  
293 profiles are visually examined and rejected.

### 294 **3 Comparison Methodology**

295 Previous studies on the validation of satellite observations used a range of coincidence criteria.  
296 Wang et al. (2011) set a 100 km radius and 3 hour time difference as coincidence criteria. Kroon  
297 et al. (2011) applied coincidence criteria of  $\pm 0.5^\circ$  for both latitude and longitude and 12 hours.  
298 In this paper, we determine our coincident criteria based on the balance between finding most  
299 coincident OMI/ozonesonde pairs to minimize differences due to spatiotemporal samplings and  
300 finding a sufficient number of pairs for statistical analysis. For each screened ozonesonde profile,  
301 we first select all filtered OMI data within  $\pm 1^\circ$  latitude,  $\pm 3^\circ$  longitude and  $\pm 6$  hours and then

302 find the nearest OMI retrieval within 100 km from the ozonesonde station to perform the  
303 validation on the individual profile basis.

304 Ozonesondes have much finer vertical resolution than OMI retrievals. To account for the  
305 different resolutions, ozonesonde profiles are first integrated into the corresponding OMI vertical  
306 grids and then degraded to the OMI vertical resolution by using the OMI retrieval Averaging  
307 Kernels (AKs) and *a priori* ozone profile based on the following equation:

$$308 \quad \hat{x} = x_a + A(x - x_a), \quad (1)$$

309 where  $x$  is the ozonesonde profile integrated into the OMI grid,  $\hat{x}$  is the retrieved ozone profile if  
310 the ozonesonde is observed by OMI,  $A$  is the OMI AK matrix, and  $x_a$  is the OMI *a priori* ozone  
311 profile. We refer to this retrieval as “convolved ozonesonde profile”, which is a reconstruction of  
312 ozonesonde profile with OMI retrieval vertical resolution and sensitivity. Missing ozone profiles  
313 above ozonesonde burst altitude are filled with OMI retrievals. The convolution process  
314 essentially removes OMI smoothing errors and the impacts of *a priori* from the comparison so  
315 that OMI/ozonesonde differences are mainly due to OMI/ozonesonde measurement precision,  
316 spatiotemporal sampling differences and other errors. However, in the regions and altitudes  
317 where OMI has low retrieval sensitivity, the comparisons can show good agreement because  
318 both the retrieval and convolved ozonesonde approach the *a priori* profile. To overcome the  
319 limitation of such a comparison, we also compare with unconvolved ozonesonde profiles since it  
320 indicates how well the retrievals can represent the actual ozonesonde observations (i.e.,  
321 smoothing errors are included as part of retrieval errors). In addition, we also compare OMI *a*  
322 *priori* and convolved/unconvolved ozonesonde profiles to indicate the retrieval improvement  
323 over the *a priori*.

324 For consistent calculations of TOC and SOC from the OMI/ozonesonde data, the tropopause  
325 pressure included in the OMI retrieval and ozonesonde burst pressure (required to be less than 12  
326 hPa or above ~30 km) are used as the proper boundaries. The TOC is integrated from the surface  
327 to the tropopause. And the SOC is not the total stratospheric ozone column, but the ozone  
328 column integrated from the tropopause pressure to the ozonesonde burst pressure.

329 The relative profile difference is calculated as (OMI- Sonde) / OMI *a priori* ×100% in the present  
330 comparison with ozonesonde and with MLS in the companion paper. Choosing OMI *a priori*

331 rather than MLS/ozonesonde is to avoid unrealistic statistics skewed by extremely small values  
332 in the reference data especially in the MLS retrievals of upper troposphere and lower  
333 stratosphere ozone (Liu et al., 2010a). Unlike the profile comparison, ozonesonde/OMI  
334 SOC/TOC values are used in the denominator in the computation of relative difference. To  
335 exclude remaining extreme outliers in the comparison statistics, values that are exceeding  $3\sigma$   
336 from the mean differences are filtered.

337 After applying the OMI/ozone filtering and coincident criteria, approximately 10,500  
338 ozonesonde profiles are used in the validation. We performed the comparison for five latitude  
339 bands: northern high latitudes ( $60^\circ$  N- $90^\circ$  N), northern mid-latitudes ( $30^\circ$  N- $60^\circ$  N), tropics ( $30^\circ$   
340 S- $30^\circ$  N), southern mid-latitudes ( $60^\circ$  S- $30^\circ$  S), and southern high latitudes ( $90^\circ$  S- $60^\circ$  S) to  
341 understand the latitudinal variation of the retrieval performance. We investigated the seasonal  
342 variations of the comparisons mainly at northern mid-latitudes where ozone retrieval shows  
343 distinct seasonality and there are adequate coincidence pairs. To investigate the RA impacts on  
344 OMI retrievals, we contrasted the comparison before (2004-2008, i.e., pre-RA) and after (2009-  
345 2014, i.e., post-RA). Although we filter OMI data based on cloud fraction, cross-track position,  
346 and SZA in the final evaluation of our retrievals against ozonesonde observations as shown in  
347 Sect. 4.1.1., we conduct the comparison as a function of these parameters using coincidences at  
348 all latitude bands to show how these parameters affect the retrieval quality as shown in the Sects.  
349 4.1.2 – 4.1.4. In these evaluations, the filtering of OMI data based on cloud fraction, cross-track  
350 position, and SZA are switched off, respectively. Approximately 15,000 additional ozonesonde  
351 profiles are used in this extended evaluation. To evaluate the long-term performance of our  
352 ozone profile retrievals, we analyze the monthly mean biases (MBs) of the OMI/ozonesonde  
353 differences as a function of time using coincidences in the  $60^\circ$  S- $60^\circ$  N region and then derive a  
354 linear trends over the entire period as well as the pre-RA and post-RA periods.

## 355 4 Results and Discussions

### 356 4.1 Comparison of Ozonesonde and OMI profiles

#### 357 4.1.1 Ozone Profile Differences

358 Comparisons of ozone profiles between OMI/a priori and ozonesondes with and without  
359 applying OMI AKs for the 10-year period (2004-2014) are shown in the left panels of Figure 3.  
360 The MBs and SDs vary spatially with altitude and latitude. Vertically, the SD typically  
361 maximizes in the upper troposphere and lower stratosphere (UTLS) in all latitude bands due to  
362 significant ozone variability and a priori uncertainty. Bak et al. (2013b) showed that the use of  
363 Tropopause-Based (TB) ozone profile climatology with NCEP Global Forecast System (GFS)  
364 daily tropopause pressure can significantly improve the a priori, and eventually reduce the  
365 retrieval uncertainty. Consequently, the SDs of OMI/sonde differences in the UTLS at mid- and  
366 high-latitudes can be reduced through reducing the retrieval uncertainties in a future version of  
367 the algorithm that uses the TB climatology. Latitudinally, the agreement is better in the tropics  
368 and becomes worse at higher latitudes. The patterns are generally similar in the northern and  
369 southern hemispheres. The MBs between OMI and ozonesonde are within ~6% with AKs and  
370 10% without AKs in the tropics and the middle latitudes. Large changes in the biases between  
371 with and without AKs occur in the tropical troposphere where the bias differences reach 10%.  
372 The MBs increase to 20-30% at high latitudes consistently with large oscillation from ~-20-30%  
373 at ~300 hPa to +20% near the surface both with and without the application of AKs. At pressure  
374 < 50 hPa, the SDs for comparisons with OMI AKs are typically 5-10% at all latitudes except for  
375 the 90° S-60° S region. For pressure > 50 hPa, the SDs are within 18% and 27% in the tropics  
376 and middle-latitudes, respectively, but increase to 40% at higher latitudes. The SDs for  
377 comparison without applying OMI AKs, i.e., including OMI smoothing errors in the  
378 OMI/ozonesonde differences, typically increase up to 5% for pressure < 50 hPa, but increase up  
379 to 15-20% for pressure > ~50hPa. The smoothing errors derived from root square differences of  
380 the MBs with and without OMI AKs are generally consistent with the retrieval estimate from the  
381 optimal estimation.

382 The improvements of OMI over the climatological (a priori) profiles can be reflected in the  
383 reduction of MBs and SDs in the comparisons between ozonesondes and OMI retrievals, and  
384 between ozonesondes and a priori. The retrieval improvements in the MBs are clearly shown in  
385 the tropics and at  $\sim 100$  hPa pressure in the middle latitudes. At high latitudes, the MBs and  
386 corresponding oscillations in the troposphere are much larger than these in the a priori  
387 comparison, suggesting that these large biases are mainly caused by other systematic  
388 measurements errors at high latitudes (larger SZAs and thus weaker signals). As can be seen  
389 from the reduction of SDs, OMI retrievals show clear improvements over the a priori at pressure  
390  $< 300$  hPa. For pressure  $> 300$  hPa, the retrieval improvements vary with latitudes. There are  
391 consistent retrieval improvements throughout the surface - 300hPa layer in the tropics and only  
392 the 550 - 300 hPa layer at middle latitude, while there is no retrieval improvement over the a  
393 priori for  $> 300$  hPa at high latitudes. The failure to improve the retrieval over a priori in part of  
394 the troposphere at middle and high latitudes is caused by several factors. They are the inherent  
395 reduction in retrieval sensitivity to lower altitudes at larger SZAs as a result of reduced photon  
396 penetration into the atmosphere, unrealized retrieval sensitivity arising from retrieval  
397 interferences with other parameters (e.g., surface albedo) as discussed in Liu et al. (2010b) and  
398 the use of floor-noise of 0.2% that underestimates the actual OMI measurement SNR. In  
399 addition, the a priori ozone error in the climatology is quite small since the SDs of the  
400 differences between the a priori and ozonesonde without AKs are typically less than 20% in the  
401 lower troposphere for middle and high latitudes, which also makes it more difficult to improve  
402 over the a priori comparison.

403 The right column of Figure 3 shows the comparisons between OMI retrievals and ozonesondes  
404 convolved with OMI AKs in the pre-RA and post-RA periods, respectively. In the tropics and  
405 mid-latitudes, the pre-RA comparison is better than the post-RA comparison, with SDs smaller  
406 by up to  $\sim 8\%$  at most altitudes especially in the troposphere. The pre-RA comparison also shows  
407 smaller biases near  $\sim 300$  hPa at middle latitudes while the post-RA comparison exhibits negative  
408 biases reaching 8-12%. At high latitudes, the pre-RA period does not show persistent  
409 improvement during the post-RA period. The pre-RA comparison shows slightly smaller SDs at  
410 most altitudes and smaller negative biases by 10% around 300 hPa in the northern high latitudes,  
411 and smaller positive biases by 20% near the surface in the southern high latitudes. The worse

412 results during the post-RA period are caused by increasingly noisy OMI measurements with  
413 smaller SNR and the additional radiometric biases made by the RA, which vary with space and  
414 time. The smaller SDs at some altitudes of high latitudes may reflect a combination of ozone  
415 variation, uneven distribution of ozonesondes with varying uncertainty at different stations, and  
416 cancellation of radiometric errors by the RA.

417 As seen from the number of OMI/ozonesonde coincidences shown in Figure 3, the northern mid-  
418 latitudes and the tropics have sufficient coincidences to validate the retrievals as a function of  
419 season. In the tropics, the retrieval comparison does exhibit little seasonality as expected (not  
420 shown). Figure 4 shows the comparison similar to Figure 3(c) for each individual season at  
421 northern middle latitudes. The comparison results are clearly season-dependent with different  
422 altitude-dependent bias patterns, and with the smallest SDs in the summer (except for the MBs)  
423 and the worst SDs in the winter. This indicates the general best retrieval sensitivity to lower  
424 tropospheric ozone during the summer as a result of small SZAs and stronger signals and worst  
425 retrieval sensitivity during the winter as a result of large SZAs and weaker signals. The MBs for  
426 with and without AKs at 300 hPa vary from ~12% in the winter to -10% in the summer. The  
427 overall MBs are the smallest during the spring, within 6%; but the MBs at pressure < 50 hPa are  
428 the best during the summer. The maximum SDs vary from 31% in the winter to 20% in the  
429 summer. Also, the retrieval in the summer shows the most improvements in terms of reduction in  
430 SDs over the a priori in the lower troposphere at all tropospheric layers except for the bottom  
431 layer, while the retrievals during other seasons show the improvement over a priori only above  
432 the lowermost two/three layers. The seasonal variation of retrieval quality is partially caused by  
433 the seasonal variations of the retrieval sensitivity and ozone variability. Bak et al. (2013b)  
434 showed that the use of TB ozone climatology with daily NCEP GFS tropopause pressure can  
435 significantly reduce the seasonal dependence of the comparison with ozonesondes. In addition,  
436 radiometric calibration errors such as those caused by stray light and RA also contribute to the  
437 seasonal variation of retrieval quality.

#### 438 **4.1.2 Solar Zenith Angle Dependence**

439 The SZA of low earth orbit (LEO) satellite observation varies latitudinally and seasonally;  
440 therefore the SZA dependence of the retrieval can cause latitudinal and seasonal dependent



441 retrieval biases. SZA is one of the main drivers that affect retrieval sensitivity especially to  
442 tropospheric ozone. At large SZA, the measured backscattered signal becomes weak due to weak  
443 incoming signal and long path length; the retrieval sensitivity to the tropospheric ozone  
444 decreases due to reduced photon penetration to the troposphere. In addition, measurements are  
445 subject to relatively larger radiometric errors such as those from stray light and as a result of  
446 weaker signal, and radiative transfer calculations can lose accuracy at larger SZA (Caudill et al.,  
447 1997).

448 Figure 5 gives the MBs and SDs of differences between OMI and ozonesondes (with OMI AKs)  
449 in a function of SZAs. We can see that retrieval performance generally becomes worse at large  
450 SZA. The SD typically increases with SZA especially at pressure > 300 hPa. At SZA larger than  
451 75°, the SD at ~300 hPa increases to greater than ~45%. The variation of MBs with SZA is more  
452 complicated. We see generally larger positive biases at larger SZA in the troposphere with >  
453 20% biases at SZA larger than 75°. The MBs near ~ 30 hPa becomes more negative at larger  
454 SZAs. There is a strip of positive biases of ~10% that slightly decreases in pressure from ~50  
455 hPa at low SZA to ~10 hPa at large SZA; it might be due to some systematic radiometric biases  
456 that can affect ozone at different altitudes varying with SZA. Because of the clear degradation of  
457 the retrieval quality at large SZA, we set the SZA filtering threshold of 75° to filter OMI data.

### 458 **4.1.3 Cloud Fraction Dependence**

459 The presence of cloud affects retrieval sensitivity since clouds typically reduce sensitivity to  
460 ozone below clouds and increase sensitivity to ozone above clouds. The accuracy of ozone  
461 retrievals is sensitive to the uncertainties of cloud information and cloud treatment (Antón and  
462 Loyola, 2011; Bak et al., 2015; Liu et al., 2010a). Our OMI ozone algorithm assumes clouds as  
463 Lambertian surfaces with optical centroid cloud pressure from the OMI Raman cloud product  
464 (Vasilkov et al., 2008), and partial clouds are modeled using independent pixel approximation  
465 such that the overall radiance is the sum of clear and cloudy radiances weighted by the effective  
466 cloud fraction. The cloud albedo is assumed to be 80% and is allowed to vary (>80%) with the  
467 effective cloud fraction.

468 Figure 6 gives the influences of effective cloud fraction on the comparisons between OMI and  
469 ozonesonde observations convolved with OMI AKs. The MBs and SDs do not change much with

470 cloud fraction for pressure < 100 hPa, and typically increase with the increase of cloud fraction  
471 for pressure > 100 hPa. The MBs at pressure > 100 hPa, especially greater~300 hPa, increase to  
472 more than 10% with cloud fraction greater than ~0.3. This indicates that the cloud fractions have  
473 small impacts on the stratospheric retrievals but large impacts on the tropospheric retrievals as  
474 expected. Some of the variation with cloud fraction such as negative biases near ~300 hPa at  
475 cloud fraction of ~0.4 and the decreases of positive biases at ~ 50 hPa for cloud fraction greater  
476 than ~0.8 may be partially related to the uncertainties of the cloud parameters. The chosen  
477 filtering threshold of 0.3 in cloud fraction is a tradeoff between validating OMI data with  
478 adequate retrieval sensitivity to tropospheric ozone and finding adequate number of  
479 OMI/ozonesonde coincidences.

#### 480 **4.1.4 Cross-Track Position Dependence**

481 The OMI swath is divided into 30 cross-track pixels at the UV1 spatial resolution of our product.  
482 Each cross-track position is measured by a different part of the CCD detector, i.e., essentially a  
483 different instrument. Radiometric calibration coefficients of the instrument are characterized  
484 during pre-launch only at selected CCD column pixels and then interpolated to other columns,  
485 causing variation in the radiometric calibration performance across the CCD detector. This in  
486 turn causes cross-track dependent biases in the calibrated radiance (Liu et al., 2010b), which  
487 therefore causes striping in almost all the OMI data products if no de-striping procedure is  
488 applied. Our retrieval algorithm has included a first-order empirical correction independent of  
489 space and time to remove the cross-track variability (Liu et al., 2010b). However, residual  
490 dependence on cross-track position remains and the radiometric calibration at different position  
491 can degrade differently with time (e.g., the RA impact). In addition, the viewing zenith angle  
492 ranges from ~0° to ~70° and the footprint area increases by approximately an order of magnitude  
493 from nadir to the first/last position. So the varying viewing zenith angle causes the variation of  
494 retrieval sensitivities and atmospheric variabilities within varying footprint areas may also cause  
495 additional cross-track dependence in the retrieval performance.

496 Figure 7 provides the MBs and SDs of the differences between OMI and ozonesonde convolved  
497 with OMI AKs as a function of cross-track position for pre-RA and post-RA periods,  
498 respectively. It clearly exhibits cross-track dependence especially with large positive/negative

499 MBs and large SDs at the first/last several extreme off-nadir positions. This is why we select  
500 cross-track positions of 4-27 in the validation to avoid positions with large biases. The enhanced  
501 biases/SDs at positions 24 (RA flagging not applied) and 27 (flagged as RA in UV2 since June  
502 25, 2007 but not flagged/applied in UV1) are due to the RA impact during the post-RA period.  
503 Cross-track positions 1-10 show consistent bias patterns with negative biases in ~300- 50 hPa  
504 layer and positive biases in ~surface – 300 hPa layer, and large standard deviation around ~ 300  
505 hPa although the magnitude decreases with increasing cross-track position. This pattern occurs  
506 during both pre-RA and post-RA periods although the values are larger during the post-RA  
507 period. For other cross-track positions, the variation is relatively smaller but we can still see  
508 small striping patterns.

## 509 **4.2 Comparison of Partial Ozone Columns**

510 We investigate and validate OMI partial ozone columns, including SOCs, TOCs, and surface-  
511 550 hPa and surface-750 hPa ozone columns in this section. We define the lowermost one and  
512 two layer as surface-750 hPa and surface-550 hPa in this paper, respectively, for conveniences.  
513 Similarly, we also analyze the validation results of SOCs and TOCs during pre-RA and post-RA,  
514 respectively, to test the impacts of RA on OMI partial ozone columns. In addition, we validate  
515 ozone columns from the surface to ~550 hPa (bottom two layers) and ~ 750 hPa (bottom one  
516 layer) against ozonesonde observations in the tropics and mid-latitude summer where there is  
517 better retrieval sensitivity to these quantities.

### 518 **4.2.1 Comparison of Stratospheric Ozone Columns (SOCs)**

519 The left column of Figure 8 shows the MBs and SDs of the comparisons of OMI and ozonesonde  
520 SOCs for each of the five latitude bands during 2004-2014. In all regions, the OMI SOCs have  
521 excellent agreement with ozonesonde SOCs regardless of whether ozonesonde data are  
522 convolved with OMI AKs. The application of OMI AKs to ozonesonde SOCs only slightly  
523 improves the comparison statistics. The MBs with OMI AKs are within 1.8% except for a  
524 negative bias of 3% at northern high latitudes, while the SDs are within 5.1% except for 5.7% at  
525 high latitudes. The correlation coefficient is greater than 0.95 except for 0.90 in the tropics due to  
526 the smaller SOC range. The SDs are typically larger than the comparisons with MLS data (Liu et

527 al., 2010a) due to worse coincidence criteria, relatively larger uncertainty in the ozonesonde  
528 stratospheric ozone columns compared to MLS data, and different altitude ranges of integration.

529 The middle and right columns of Figure 8 show comparison results during the pre-RA and post-  
530 RA periods, respectively. The comparison is typically better during the pre-RA with SDs smaller  
531 by 0.2-0.6% and larger correlation coefficients although the MBs are generally smaller during  
532 the post-RA period. One exception is at southern high-latitudes where the post-RA comparison  
533 statistics are significantly better except for the MB, consistent with Figure 3, likely due to a  
534 combination of ozone variation between these two periods, uneven distribution of ozonesondes  
535 at different stations, and cancellation of various calibration errors.

#### 536 **4.2.2 Comparison of Partial Ozone Columns in the Troposphere**

537 The left column of Figure 9 shows the comparison of OMI and ozonesonde (with and without  
538 OMI AKs) TOCs for each of the five latitude bands during 2004-2014. Without applying OMI  
539 AKs, the MBs are within 1-3% except for 9% at northern high latitudes; The SDs are within 20%  
540 in the tropics and mid-latitudes and increase to ~30-40% at high-latitudes. The correlation  
541 coefficient ranges from 0.83 in the tropics to ~0.7 at middle latitudes, and 0.5-0.6 at high-  
542 latitudes. The linear regression slopes are in the range 0.6-0.8 typically smaller at high latitudes  
543 due to reduced retrieval sensitivity to the lower troposphere. After applying the OMI AKs to  
544 ozonesonde data to remove smoothing errors, we see significant improvement in the comparison  
545 statistics except for MBs, which are within 6% at all latitudes. The SDs are reduced to within  
546 15% in the tropics and middle latitudes and ~30% (5.5-8.1 DU) at high latitudes; the correlation  
547 improves by 0.04-0.12 and the slope significantly increases by 0.12-0.23 to the range 0.8-1.0 at  
548 different latitude bands due to accounting for inadequate retrieval sensitivity to the lower and  
549 middle troposphere.

550 The middle and right columns of Figure 9 show comparisons during pre-RA and post-RA,  
551 respectively. The comparison between OMI and ozonesondes with OMI AKs TOCs during the  
552 pre-RA period is significantly better than these during the post-RA period in the tropics and mid-  
553 latitudes with SDs smaller by 3.4-5.5% and greater correlation. The MBs during the post-RA  
554 period is smaller by ~2 DU at mid-latitudes, but larger by ~1 DU in the tropics. However, the

555 post-RA comparison is similar to the pre-RA comparison at northern high-latitudes and is even  
556 better at southern high latitudes probably due to the aforementioned ozonesonde issues.

557 Figure 10 shows examples of time series when comparing individual OMI and ozonesondes  
558 (with OMI AKs) TOCs and their corresponding differences at six selected stations, one for each  
559 latitude region of 90° N-60° N, 60° N-30° N, 30° N-0°, 0°-30° S, 30° S-60° S and 60° S-90° S.  
560 OMI TOC shows good agreement with ozonesondes at these stations with overall MBs  $\leq 3$  DU  
561 and SDs less than 5.1 DU. The comparison is also good even in the high latitude regions partially  
562 because the Summit and Neymayer stations only have ozonesonde launches during local  
563 summer. Seasonal dependent biases are clearly seen at Payerne, and bias trends can be seen at  
564 several stations with positive trends at Summit and Neumayer and a negative trend at Naha. In  
565 the pre-RA and post-RA periods, the MBs are typically within 2 DU and the SDs are typically  
566 smaller during the pre-RA period except for Naha. The better comparison (both mean bias and  
567 standard deviation) during the post-RA period at Naha is likely due to the switch to ECC  
568 ozonesondes beginning on November 13, 2008 from KC ozonesonde that have greater  
569 uncertainty (WMO, 1998).

570 Figure 2 also shows the MBs and SDs of the TOC differences between OMI and ozonesonde  
571 convolved with OMI AKs at each station/location where there are at least 10 coincident  
572 OMI/ozonesonde pairs. OMI data generally exhibit good agreement with ozonesondes at most of  
573 the stations, with MBs of  $\leq 3$  DU and SDs of  $\leq 6$  DU. In the tropics (30° S-30° N), very large  
574 SDs ( $>11$  DU) occur at the two Indian stations (New Delhi, and Trivandrum). In addition, there  
575 is a large bias of  $> 6$  DU at New Delhi. The poor comparisons at these two stations are likely  
576 associated with the large uncertainties of the Indian ozonesonde data. Hilo has large biases of  
577  $\sim 4.5$  DU with 3.2 and 6.2 DU for pre-RA and post-RA, respectively. Java also has a large bias of  
578  $\sim 5$  DU but shows little difference between pre-RA and post-RA. Consistent  $\sim 2\%$  and  $\sim 5\%$   
579 underestimates of OC by ozonesondes compared to OMI total ozone are found in Hilo and Java,  
580 respectively (Thompson et al., 2012). These OC underestimates may partly explain the large  
581 TOC biases in Hilo and Java. However, the reason for underestimates of ozonesonde-derived OC  
582 is unknown. In the middle latitudes, noticeably large SDs and/or biases occur at a few stations  
583 such as Churchill, Sable Islands, Hohenpeissenberg, and Parah. Three Japanese stations,  
584 Sapporo, Tateno, and Naha, exhibit relatively large biases of 2-3 DU and even larger biases

585 before switching from KC to ECC sondes. Almost half of the 11 northern high latitude stations  
586 ( $60^{\circ}$  N- $90^{\circ}$  N) and two of the 6 southern high-latitude stations have large SDs/biases. In addition  
587 to retrieval biases from the OMI data, some of the large biases or SDs might be partially related  
588 to ozonesonde type with different biases and uncertainties due to different types (e.g., Indian  
589 sonde stations, Brewer-Mast ozonesonde at Hohenpeissenberg, three KC sonde stations),  
590 manufacturers (e.g., SP vs. ENSCI for ECC sonde), sensor solution or related to individual sonde  
591 operations, which was shown in the validation of GOME ozone profile retrievals (Liu et al.,  
592 2006a).

593 Figure 11 shows the comparison for each season at northern mid-latitudes. Consistent with  
594 profile comparison, the TOC comparison is season-dependent. When applying OMI AKs, the  
595 mean bias varies from 3 DU in winter to -1.5 DU in summer. The SDs are within 6.8 DU with  
596 the smallest value during fall due to less ozone variability. The regression slopes are very close,  
597 within 0.04 around 0.67. The retrieval sensitivity is smallest during the summer as seen from the  
598 greatest correlation and slope and relatively small standard deviation, and is the worst during the  
599 winter. With OMI AKs applied to ozonesonde profiles, the MBs only slightly change (varying  
600 from 3.5 DU to -1.3 DU), but the SDs are significantly reduced to within 5.2 DU, the slopes  
601 significantly increase by  $\sim 0.2$  to 0.8-1.0, and the correlation improves significantly during the  
602 winter and spring.

603 Figure 12 compares the surface $\sim$ 550 hPa and surface $\sim$ 750 hPa ozone columns with ozonesonde  
604 data in the middle latitudes during summer and the tropics. Compared to the TOC comparisons  
605 in Figure 9 and Figure 11, the comparisons of these lower tropospheric ozone columns exhibit  
606 smaller regression slopes and correlations that are a result of reduced retrieval sensitivity. In the  
607 tropics, the slopes decrease from 0.78 in TOC to 0.65 in the surface $\sim$ 550 hPa ozone column and  
608  $\sim 0.50$  in the surface $\sim$ 750 hPa column, with corresponding correlation from 0.83 to 0.74 in the  
609 surface $\sim$ 550 hPa column, and 0.66 in the surface $\sim$ 750 hPa column. This indicates that the  
610 retrievals in the surface $\sim$ 550 hPa/750 hPa can capture  $\sim 65\%/50\%$  of the actual ozone change  
611 from the a priori. During the middle latitude summer, the slope decreases from 0.71 in the TOC  
612 comparisons to 0.42 in the surface $\sim$ 550 hPa comparisons and 0.32 in the surface $\sim$ 750 hPa  
613 comparisons, with corresponding correlation coefficients from 0.74 to 0.5 and 0.46. Thus, the  
614 retrievals in the surface $\sim$ 550 hPa and  $\sim$ 750 hPa only capture  $\sim 40\%/30\%$  of the actual ozone

615 change from the a priori. The MBs are generally small within 0.5 DU (5%) with SDs of ~3.6 DU  
616 (20-28%) in the surface~550 hPa ozone column and ~2.5 DU (25-36%) in the surface~750 hPa  
617 ozone column. After applying OMI AKs to account for inadequate retrieval sensitivity and  
618 removing smoothing errors, the slope significantly increases to approach 1 (as expected). SDs  
619 are reduced to ~10% in the middle latitudes and ~15% in the tropics.

### 620 **4.3 Evaluation of Long-term Performance**

621 Comparisons in Sects 4.1 and 4.2 indicated systematic differences between pre-RA and post-RA  
622 periods and generally worse performance during the post-RA periods. To further illustrate the  
623 long-term stability of our ozone profile product and understand the quality of OMI radiometric  
624 calibration as a function of time, we analyze monthly MBs of OMI/ozonesonde differences with  
625 OMI retrieval AKs in ozone profiles, SOCs, and TOCs. Due to the lack of OMI observations  
626 during some months at high-latitudes, we focus the evaluation by using coincidence pairs in 60°  
627 S-60° N. Monthly MBs are calculated only if there are more than 5 OMI-ozonesonde pairs in a  
628 given month. Linear regression trend is on the MBs for the entire period (2004-2014) and/or for  
629 the pre-RA and post-RA periods, respectively. The trend is considered statistically significant if  
630 its P value is less than 0.05.

631 The linear trends of monthly mean ozone biases for each OMI layer between 60° S-60° N are  
632 plotted in Figure 13 for each of the three periods. During 2004-2014, marked in black, ozone  
633 biases at layers above 50.25 hPa show significant positive trends of 0.06-0.17 DU/year (0.17-  
634 0.52%/year), while ozone biases between 290 hPa and 110 hPa exhibit significant negative  
635 trends of 0.1-0.19 DU/year (1-2%/year). The positive trends in the stratosphere are generally  
636 consistent with those shown in OMI-MLS comparisons (Huang et al., 2017). In the lowermost  
637 three OMI layers, ozone differences are more stable but with several large spikes during the post-  
638 RA periods likely due to the RA evolution or instrument operation. The derived trends for the  
639 pre-RA period are generally more flat and insignificant at all layers indicating good stability of  
640 our product as well as the OMI radiometric calibration. During the post-RA period, the derived  
641 trends are positive above 75 hPa with statistical significance. These positive trends in the  
642 stratosphere are generally similar to those over the entire period, suggesting the dominant  
643 contribution of the post-RA period to the overall trend. In the altitude range 214 – 108 hPa, the

644 post-RA trends are also flat similar to the pre-RA trends, but the values are systematically  
645 smaller during the post-RA period, causing significantly negative trends over the entire period.

646 The SOC biases exhibit small positive trend of  $0.14 \pm 0.09$  DU/year in 2004-2014 with no  
647 statistical significance (Figure 14(a)). This slight positive trend is a result of trend cancellation  
648 by the positive trends above 80 hPa and negative trends between 220 hPa and 80 hPa The TOC  
649 biases reveal a significant negative trend of  $-0.18 \pm 0.05$  DU/year (Figure 14(b)), mostly from  
650 layers in the upper troposphere. In the pre-RA and post-RA periods, both trends of both SOC and  
651 TOC biases are relatively flat during the pre-RA period, while the SOC trend in the post-RA  
652 period is  $0.77 \pm 0.20$  DU/year with significance. It is noticeable that the P value of TOC trend in  
653 the post-RA period is 0.06.

654 The significant trends of ozone biases at different layers as well as in SOC and TOC suggest that  
655 the current ozone profile product is not suitable for trend studies especially during the post-RA  
656 period. The relatively flat bias trends during the pre-RA periods and statistically significant  
657 trends during the post-RA period confirm that the better stability of our product during the pre-  
658 RA period and more temporal variation of the retrieval performance during the post-RA period  
659 are likely associated with the RA evolution. In previous sections, the validation of our retrievals  
660 revealed latitudinal/seasonal/SZA and cross-track dependent biases even during the pre-RA  
661 period. This indicates the need to remove signal dependent errors and the calibration  
662 inconsistency across the track. To maintain the spatial consistency and long-term stability of our  
663 ozone profile product, we need to further improve OMI's radiometric calibration especially  
664 during the post-RA period. Preferably, the calibration improvement should be done in the level  
665 0-1b processing. If this option is not possible, we can perform soft calibration similar to Liu et al.  
666 (2010b) but derive the correction as a function of time and latitude/SZA. In addition, it should be  
667 noted that the trend calculation might be affected by factors such as the availability of correction  
668 factors with ozonesondes (Morris et al., 2013), station-to-station variability and the uneven  
669 spatiotemporal distribution of the ozonesondes, which can introduce considerable sampling  
670 biases (Liu et al., 2009; Saunois et al., 2012).



## 671 **5 Summary and Conclusion**

672 We conducted a comprehensive evaluation of the quality of OMI ozone profile (PROFOZ)  
673 products produced by the SAO algorithm, including their spatial consistency and long-term  
674 performance using coincident global ozonesonde observations during the decade 2004-2014. To  
675 better understand retrieval errors and sensitivity, we compared the retrieved ozone profiles and a  
676 priori profile at individual layers with ozonesondes before and after being degraded to the OMI  
677 vertical resolution with OMI retrieval average kernels (AKs). We also compared the integrated  
678 SOC, TOC, and surface-~550/~750 hPa ozone columns with ozonesonde data. To understand the  
679 spatial distribution of retrieval performance, the validations are grouped into five latitude ranges:  
680 northern/southern high/middle latitudes, and the tropics. To investigate the impacts of the OMI  
681 row anomaly (RA) on the retrievals, we contrasted the comparison before and after the  
682 occurrence of major OMI RA in January 2009, i.e., pre-RA (2004-2008) and post-RA (2009-  
683 2014) periods. In addition, we quantified the dependence of retrieval performance on seasonality  
684 and several key parameters including solar zenith angle (SZA), cloud fraction, and cross-track  
685 position. Finally, we analyzed the monthly mean variation of the mean biases (MBs) to examine  
686 the long-term stability of the PROFOZ product.

687 The comparison between OMI and ozonesonde profiles varies in altitude, with maximum  
688 standard deviations (SDs) in the Upper Troposphere and Lower Stratosphere (UTLS) due to  
689 significant ozone variability, and varies with latitude similarly in the northern and southern  
690 hemispheres. There is good agreement throughout the atmosphere in the tropics and mid-  
691 latitudes. With the application of OMI AKs to ozonesonde data, the MBs are within 6%, and the  
692 SDs increase from 5-10% for pressure < ~50 hPa to within 18%(27%) in the tropics/mid-  
693 latitudes for pressure > ~50 hPa. In the high latitudes, the retrievals agree well with ozonesondes  
694 only for pressure < ~50 hPa with MBs of < 10% and SDs of 5-15% for pressure < ~ 50 hPa, but  
695 with MBs reaching 30% and SDs reaching 40% for pressure > ~50 hPa. The comparison results  
696 are seasonally dependent. At northern mid-latitudes, there are generally the best retrieval  
697 sensitivity and the smallest SDs as great as 20% in the summer, and the worst sensitivity and the  
698 largest SDs reaching 31% in the winter. The MBs near 300 hPa vary from 12% in the winter to -  
699 10% in the summer. The post-RA comparison is generally worse in the tropics and mid-latitudes  
700 than the pre-RA comparison, with SDs larger by up to 8% in the troposphere and 2% in the

701 stratosphere, and with larger MBs around ~300 hPa in the mid-latitudes. But at high latitudes, the  
702 pre-RA comparison does not show persistent improvement over the post-RA comparison, with  
703 smaller biases and larger SDs at some altitudes, especially at southern high latitudes. The  
704 retrieval improvement over a priori can be determined from the SD reduction of the retrieval  
705 comparison from the a priori comparison. The retrievals demonstrate clear improvement over the  
706 a priori down to the surface in the tropics, but only down to ~750 hPa during mid-latitude  
707 summer, ~550 hPa during the other seasons of mid-latitudes and ~ 300 hPa at high latitudes.

708 Retrieval performance typically becomes worse at large SZA, especially at SZA larger than 75°,  
709 where the MBs in the troposphere are >20% and the SDs near ~300 hPa are > 45%. The worse  
710 performance at larger SZA is due to a combination of weaker signal and greater influence by  
711 radiometric calibration errors such as due to stray light, and radiative transfer calculation errors.  
712 The variation of SZA is likely responsible for the majority of the retrieval dependence on latitude  
713 and season. The retrieval quality for pressure > ~100 hPa degrades with increasing cloudiness in  
714 terms of MBs and SDs, with MBs greater than 10% at cloud fraction > 0.3. The retrieval  
715 performance also varies with cross-track position, especially with large MBs and SDs at the  
716 first/last extreme off-nadir positions (e.g., 1-3 and 28-30). The dependence is stronger during the  
717 post-RA period.

718 The integrated SOC<sub>s</sub> and TOC<sub>s</sub> also exhibit good agreement with ozonesondes. With the  
719 convolution of OMI AKs to ozonesonde data, the SOC MBs are within 2% with SDs within  
720 ~5.1% in the tropics and mid-latitudes. These statistics do not change much even without the  
721 applications of OMI AKs. The comparison becomes slightly worse at high latitudes, with MBs  
722 up to 3% and SDs up to 6%. The pre-RA comparison is generally better with smaller SDs of 0.2-  
723 0.6% except for southern high latitudes, although with slightly larger MBs. The TOC MBs and  
724 SDs with OMI AKs are within 6%, with SDs of <~15% in the tropics and mid-latitudes but reach  
725 30% at high latitudes. The pre-RA TOC comparison is also better in the tropics and mid-latitudes  
726 with SDs smaller by 3.4-5.5% but worse values at southern high latitudes. The TOC comparison  
727 at northern mid-latitudes varies with season, with MBs of 11%. There are worse correlation  
728 during winter and MBs of -3% and best correlation in summer. The TOC comparison also shows  
729 noticeable station-to-station variability in similar latitude ranges with much larger MBs and/or  
730 SDs at the two Indian stations and larger MBs at several Japanese stations before they switched

731 from KC ozonesondes to ECC ozonesondes. This demonstrates the impacts of ozonesonde  
732 uncertainties due to sonde types, manufacturers, sensor solution and operations. Without  
733 applying OMI AKs, the TOC correlation with ozonesondes typically becomes worse at higher  
734 latitudes, ranging from 0.83 in the tropics to 0.5-0.6 at high latitudes. The linear regression slope  
735 is within 0.6-0.8, typically smaller at higher latitudes, reflecting the smaller retrieval sensitivity  
736 down to the troposphere at higher latitudes mainly resulting from larger SZA. The convolution of  
737 AKs significantly improves the correlation and slope. The impact of retrieval sensitivity related  
738 to SZA is also reflected in the seasonal dependence of the comparison at mid-latitudes.

739 The surface-~550/750 hPa ozone columns in the tropics during mid-latitude summer compare  
740 quite well with ozonesonde data, with MBs of < 5% and SDs of 20-25%/28-36% without OMI  
741 AKs. The correlation and slope decrease with decreasing altitude range due to reduced retrieval  
742 sensitivity down to the lower troposphere. These columns capture ~65%/50% of the actual ozone  
743 change in the tropics and ~40%/30% in the troposphere. Convoluting ozonesonde data with OMI  
744 AKs significantly increases the slope to ~1 and reduce the SDs to 10-15%.

745 The contrast of pre-RA and post-RA comparisons indicates generally worse post-RA  
746 performance with larger SDs. Linear trend analysis of the OMI/ozonesonde monthly MBs further  
747 reveals additional RA impact. The temporal performance over 60° S-60° N is generally stable  
748 with no statistically significant trend during the pre-RA period, but displays a statistically  
749 significant trend of 0.14-0.7%/year at individual layers for pressure < ~80 hPa, 0.7 DU/year in  
750 SOC and -0.33 DU/year in TOC during the post-RA period. Because of these artificial trends in  
751 our product, we caution against using our product for ozone trend studies.

752 This validation study demonstrates generally good retrieval performance of our ozone profile  
753 product especially in the tropics and mid-latitudes during the pre-RA period. However, the  
754 spatiotemporal variation of retrieval performance suggests that OMI's radiometric calibration  
755 should be improved, especially during the post-RA period, including the removal of signal-  
756 dependent errors, calibration inconsistency across the track and with time to maintain the long-  
757 term stability and spatial consistency of our ozone profile product.

758

759 **Acknowledgements**

760 This study was supported by the NASA Atmospheric Composition: Aura Science Team  
761 (NNX14AF16G) and the Smithsonian Institution. The Dutch-Finnish OMI instrument is part of  
762 the NASA EOS Aura satellite payload. The OMI Project is managed by NIVR and KNMI in the  
763 Netherlands. We acknowledge the OMI International Science Team for producing OMI data. We  
764 also acknowledge the ozonesonde providers and their funding agencies for making ozonesonde  
765 measurements, and the Aura Validation Data Center (AVDC), WOUDC, SHADOZ,  
766 DISCOVER-AQ, and SEACR<sup>4</sup>S for archiving the ozonesonde data.

767 **References**

- 768 Antón, M., and Loyola, D.: Influence of cloud properties on satellite total ozone observations, *J.*  
769 *Geophys. Res.*, 116, doi: 10.1029/2010JD014780, 2011.
- 770 Bak, J., Kim, J. H., Liu, X., Chance, K., and Kim, J.: Evaluation of ozone profile and  
771 tropospheric ozone retrievals from GEMS and OMI spectra, *Atmos. Meas. Tech.*, 6, 239-249,  
772 2013a.
- 773 Bak, J., Liu, X., Kim, J. H., Chance, K., and Haffner, D. P.: Validation of OMI total ozone  
774 retrievals from the SAO ozone profile algorithm and three operational algorithms with Brewer  
775 measurements, *Atmos. Chem. Phys.*, 15, 667-683, doi: 10.5194/acp-15-667-2015, 2015.
- 776 Bak, J., Liu, X., Wei, J. C., Pan, L. L., Chance, K., and Kim, J. H.: Improvement of OMI ozone  
777 profile retrievals in the upper troposphere and lower stratosphere by the use of a tropopause-  
778 based ozone profile climatology, *Atmos. Meas. Tech.*, 6, 2239-2254, doi: 10.5194/amt-6-2239-  
779 2013, 2013b.
- 780 Bhartia, P. K., and Wellemeyer, C. G.: TOMS-V8 total ozone algorithm, in: *OMI Algorithm*  
781 *Theoretical Basis Document*, edited by: Bhartia, P. K., Greenbelt, 2002.
- 782 Cai, Z., Liu, Y., Liu, X., Chance, K., Nowlan, C. R., Lang, R., Munro, R., and Suleiman, R.:  
783 Characterization and correction of Global Ozone Monitoring Experiment 2 ultraviolet  
784 measurements and application to ozone profile retrievals, *J. Geophys. Res.*, 117, doi:  
785 10.1029/2011jd017096, 2012.
- 786 Caudill, T. R., Flittner, D. E., Herman, B. M., Torres, O., and McPeters, R. D.: Evaluation of the  
787 pseudo-spherical approximation for backscattered ultraviolet radiances and ozone retrieval, *J.*  
788 *Geophys. Res.*, 102, 3881-3890, 1997.
- 789 Claas, J.: *OMI and AURA: Status, Instrument, Spacecraft and Operations*, OMI Science Meeting  
790 Meeting, De Bilt, the Netherlands, 2014.
- 791 Deshler, T., Mercer, J. L., Smit, H. G. J., Stubi, R., Levrat, G., Johnson, B. J., Oltmans, S. J.,  
792 Kivi, R., Thompson, A. M., Witte, J., Davies, J., Schmidlin, F. J., Brothers, G., and Sasaki, T.:  
793 Atmospheric comparison of electrochemical cell ozonesondes from different manufacturers, and  
794 with different cathode solution strengths: The Balloon Experiment on Standards for  
795 Ozonesondes, *J. Geophys. Res.*, 113, doi: 10.1029/2007JD008975, 2008.
- 796 Hassler, B., Petropavlovskikh, I., Staehelin, J., August, T., Bhartia, P. K., Clerbaux, C.,  
797 Degenstein, D., Mazière, M. D., Dinelli, B. M., Dudhia, A., Dufour, G., Frith, S. M., Froidevaux,  
798 L., Godin-Beekmann, S., Granville, J., Harris, N. R. P., Hoppel, K., Hubert, D., Kasai, Y.,  
799 Kurylo, M. J., Kyrölä, E., Lambert, J. C., Levelt, P. F., McElroy, C. T., McPeters, R. D., Munro,  
800 R., Nakajima, H., Parrish, A., Raspollini, P., Remsberg, E. E., Rosenlof, K. H., Rozanov, A.,  
801 Sano, T., Sasano, Y., Shiotani, M., Smit, H. G. J., Stiller, G., Tamminen, J., Tarasick, D. W.,  
802 Urban, J., van der A, R. J., Veefkind, J. P., Vigouroux, C., von Clarmann, T., von Savigny, C.,  
803 Walker, K. A., Weber, M., Wild, J., and Zawodny, J. M.: Past changes in the vertical distribution  
804 of ozone - Part 1: Measurement techniques, uncertainties and availability, *Atmos. Meas. Tech.*,  
805 7, 1395-1427, doi: 10.5194/amt-7-1395-2014, 2014.

806 Hayashida, S., Liu, X., Ono, A., Yang, K., and Chance, K.: Observation of ozone enhancement  
807 in the lower troposphere over East Asia from a space-borne ultraviolet spectrometer, *Atmos.*  
808 *Chem. Phys.*, 15, 9865-9881, doi: 10.5194/acp-15-9865-2015, 2015.

809 Huang, G., Liu, X., Chance, K., Yang, K., and Cai, Z.: Validation of 10-year SAO OMI Ozone  
810 Profile (PROFOZ) Product Using Aura MLS Measurements, *Atmos. Meas. Tech. Discuss.*,  
811 2017, 1-25, doi: 10.5194/amt-2017-92, 2017.

812 Huang, G., Newchurch, M. J., Kuang, S., Buckley, P. I., Cantrell, W., and Wang, L.: Definition  
813 and determination of ozone laminae using Continuous Wavelet Transform (CWT) analysis,  
814 *Atmos. Environ.*, 104, 125-131, doi: 10.1016/j.atmosenv.2014.12.027, 2015.

815 Johnson, B. J.: Electrochemical concentration cell (ECC) ozonesonde pump efficiency  
816 measurements and tests on the sensitivity to ozone of buffered and unbuffered ECC sensor  
817 cathode solutions, *IEEE T. Geosci. Remote.*, 107, 4393, doi: 10.1029/2001jd000557, 2002.

818 Kim, P. S., Jacob, D. J., Liu, X., Warner, J. X., Yang, K., Chance, K., Thouret, V., and Nedelec,  
819 P.: Global ozone–CO correlations from OMI and AIRS: constraints on tropospheric ozone  
820 sources, *Atmos. Chem. Phys.*, 13, 9321-9335, doi: 10.5194/acp-13-9321-2013, 2013.

821 Kivi, R., Kyrö, E., Turunen, T., Harris, N. R. P., von der Gathen, P., Rex, M., Andersen, S. B.,  
822 and Wohltmann, I.: Ozonesonde observations in the Arctic during 1989–2003: Ozone variability  
823 and trends in the lower stratosphere and free troposphere, *J. Geophys. Res.*, 112, doi:  
824 10.1029/2006JD007271, 2007.

825 Komhyr, W. D.: Operations on handbook-Ozone measurements to 40-km altitude with model 4A  
826 electrochemical concentration cell (ECC) ozonesondes, NOAA Tech. Memo. ERLARL-149 Air  
827 Resour. Lab., Boulder, CO, 49 pp., 1986.

828 Komhyr, W. D., Connor, B. J., McDermid, I. S., McGee, T. J., Parrish, A. D., and Margitan, J. J.:  
829 Comparison of STOIC 1989 ground-based lidar, microwave spectrometer, and Dobson  
830 spectrophotometer Umkehr ozone profiles with ozone profiles from balloon-borne  
831 electrochemical concentration cell ozonesondes, *J. Geophys. Res.*, 100, 9273-9282, 1995.

832 Kroon, M., de Haan, J. F., Veeffkind, J. P., Froidevaux, L., Wang, R., Kivi, R., and Hakkarainen,  
833 J. J.: Validation of operational ozone profiles from the Ozone Monitoring Instrument, *J.*  
834 *Geophys. Res.*, 116, D18305, doi: 10.1029/2010jd015100, 2011.

835 Lal, S., Venkataramani, S., Srivastava, S., Gupta, S., Mallik, C., Naja, M., Sarangi, T., Acharya,  
836 Y. B., and Liu, X.: Transport effects on the vertical distribution of tropospheric ozone over the  
837 tropical marine regions surrounding India, *J. Geophys. Res.*, 118, 1513-1524, 2013.

838 Levelt, P. F., van den Oord, G. H. J., Dobber, M. R., Malkki, A., Visser, H., de Vries, J.,  
839 Stammes, P., Lundell, J. O. V., and Saari, H.: The Ozone Monitoring Instrument, *IEEE T.*  
840 *Geosci. Remote.*, 44, 1093-1101, 2006.

841 Liu, G., Liu, J., Tarasick, D. W., Fioletov, V. E., Jin, J. J., Moeini, O., Liu, X., Sioris, C. E., and  
842 Osman, M.: A global tropospheric ozone climatology from trajectory-mapped ozone soundings,  
843 *Atmos. Chem. Phys.*, 13, 10659-10675, doi: 10.5194/acp-13-10659-2013, 2013.

844 Liu, G., Tarasick, D. W., Fioletov, V. E., Sioris, C. E., and Rochon, Y. J.: Ozone correlation  
845 lengths and measurement uncertainties from analysis of historical ozonesonde data in North  
846 America and Europe, *J. Geophys. Res.*, 114, doi: 10.1029/2008JD010576, 2009.

847 Liu, X., Bhartia, P. K., Chance, K., Froidevaux, L., Spurr, R. J. D., and Kurosu, T. P.: Validation  
848 of Ozone Monitoring Instrument (OMI) ozone profiles and stratospheric ozone columns with  
849 Microwave Limb Sounder (MLS) measurements, *Atmos. Chem. Phys.*, 10, 2539-2549, doi:  
850 10.5194/acp-10-2539-2010, 2010a.

851 Liu, X., Bhartia, P. K., Chance, K., Spurr, R. J. D., and Kurosu, T. P.: Ozone profile retrievals  
852 from the Ozone Monitoring Instrument, *Atmos. Chem. Phys.*, 10, 2521-2537, doi: 10.5194/acp-  
853 10-2521-2010, 2010b.

854 Liu, X., Chance, K., and Kurosu, T. P.: Improved ozone profile retrievals from GOME data with  
855 degradation correction in reflectance, *Atmos. Chem. Phys.*, 7, 1575-1583, 2007.

856 Liu, X., Chance, K., Sioris, C. E., Kurosu, T. P., and Newchurch, M. J.: Intercomparison of  
857 GOME, ozonesonde, and SAGE II measurements of ozone: Demonstration of the need to  
858 homogenize available ozonesonde data sets, *J. Geophys. Res.*, 111, D114305, doi:  
859 10.1029/2005jd006718, 2006a.

860 Liu, X., Chance, K., Sioris, C. E., Kurosu, T. P., Spurr, R. J. D., Martin, R. V., Fu, T.-M., Logan,  
861 J. A., Jacob, D. J., Palmer, P. I., Newchurch, M. J., Megretskaiia, I. A., and Chatfield, R. B.: First  
862 directly retrieved global distribution of tropospheric column ozone from GOME: Comparison  
863 with the GEOS-CHEM model, *J. Geophys. Res.*, 111, doi: 10.1029/2005JD006564, 2006b.

864 Liu, X., Chance, K., Sioris, C. E., Spurr, R. J. D., Kurosu, T. P., Martin, R. V., and Newchurch,  
865 M. J.: Ozone profile and tropospheric ozone retrievals from the Global Ozone Monitoring  
866 Experiment: Algorithm description and validation, *J. Geophys. Res.*, 110, D20307, doi:  
867 10.1029/2005jd006240, 2005.

868 McPeters, R. D., Labow, G. J., and Logan, J. A.: Ozone climatological profiles for satellite  
869 retrieval algorithms, *J. Geophys. Res.*, 112, D05308, doi: 10.1029/2005jd006823, 2007.

870 Morris, G. A., Labow, G., Akimoto, H., Takigawa, M., Fujiwara, M., Hasebe, F., Hirokawa, J.,  
871 and Koide, T.: On the use of the correction factor with Japanese ozonesonde data, *Atmos. Chem.*  
872 *Phys.*, 13, 1243-1260, doi: 10.5194/acp-13-1243-2013, 2013.

873 Pittman, J. V., Pan, L. L., Wei, J. C., Irion, F. W., Liu, X., Maddy, E. S., Barnett, C. D., Chance,  
874 K., and Gao, R.-S.: Evaluation of AIRS, IASI, and OMI ozone profile retrievals in the  
875 extratropical tropopause region using in situ aircraft measurements, *J. Geophys. Res.*, 114,  
876 24109, doi: 10.1029/2009jd012493, 2009.

877 Saunio, M., Emmons, L., Lamarque, J. F., Tilmes, S., Wespes, C., Thouret, V., and Schultz, M.:  
878 Impact of sampling frequency in the analysis of tropospheric ozone observations, *Atmos. Chem.*  
879 *Phys.*, 12, 6757-6773, doi: 10.5194/acp-12-6757-2012, 2012.

880 Sellitto, P., Bojkov, B. R., Liu, X., Chance, K., and Del Frate, F.: Tropospheric ozone column  
881 retrieval at northern mid-latitudes from the Ozone Monitoring Instrument by means of a neural  
882 network algorithm, *Atmospheric Measurement Techniques*, 4, 2375-2388, 2011.

883 Smit, H. G. J., Straeter, W., Johnson, B. J., Oltmans, S. J., Davies, J., Tarasick, D. W., Hoegger,  
884 B., Stubi, R., Schmidlin, F. J., Northam, T., Thompson, A. M., Witte, J. C., Boyd, I., and Posny,  
885 F.: Assessment of the performance of ECC-ozonesondes under quasi-flight conditions in the  
886 environmental simulation chamber: Insights from the Juelich Ozone Sonde Intercomparison  
887 Experiment (JOSIE), *J. Geophys. Res.*, 112, 19306, 2007.

888 Tarasick, D. W., Jin, J. J., Fioletov, V. E., Liu, G., Thompson, A. M., Oltmans, S. J., Liu, J.,  
889 Sioris, C. E., Liu, X., Cooper, O. R., Dann, T., and Thouret, V.: High-resolution tropospheric  
890 ozone fields for INTEX and ARCTAS from IONS ozonesondes, *J. Geophys. Res.*, 115, 20301,  
891 doi: doi: 10.1029/2009JD012918, 2010.

892 Thompson, A. M., Miller, S. K., Tilmes, S., Kollonige, D. W., Witte, J. C., Oltmans, S. J.,  
893 Johnson, B. J., Fujiwara, M., Schmidlin, F. J., Coetzee, G. J. R., Komala, N., Maata, M., bt  
894 Mohamad, M., Nguyo, J., Mutai, C., Ogino, S. Y., Da Silva, F. R., Leme, N. M. P., Posny, F.,  
895 Scheele, R., Selkirk, H. B., Shiotani, M., Stübi, R., Levrat, G., Calpini, B., Thouret, V., Tsuruta,  
896 H., Canossa, J. V., Vömel, H., Yonemura, S., Diaz, J. A., Tan Thanh, N. T., and Thuy Ha, H. T.:  
897 Southern Hemisphere Additional Ozonesondes (SHADOZ) ozone climatology (2005-2009):  
898 Tropospheric and tropical tropopause layer (TTL) profiles with comparisons to OMI-based  
899 ozone products, *J. Geophys. Res.*, 117, doi: 10.1029/2011jd016911, 2012.

900 Thompson, A. M., Stauffer, R. M., Miller, S. K., Martins, D. K., Joseph, E., Weinheimer, A. J.,  
901 and Diskin, G. S.: Ozone profiles in the Baltimore-Washington region (2006-2011): satellite  
902 comparisons and DISCOVER-AQ observations, *J Atmos Chem*, 72, 393-422, doi:  
903 10.1007/s10874-014-9283-z, 2015.

904 Thompson, A. M., Stone, J. B., Witte, J. C., Miller, S. K., Oltmans, S. J., Kucsera, T. L., Ross,  
905 K. L., Pickering, K. E., Merrill, J. T., Forbes, G., Tarasick, D. W., Joseph, E., Schmidlin, F. J.,  
906 McMillan, W. W., Warner, J., Hints, E. J., and Johnson, J. E.: Intercontinental Chemical  
907 Transport Experiment Ozonesonde Network Study (IONS) 2004: 2. Tropospheric ozone budgets  
908 and variability over northeastern North America, *J. Geophys. Res.*, 112, doi:  
909 10.1029/2006jd007670, 2007a.

910 Thompson, A. M., Stone, J. B., Witte, J. C., Miller, S. K., Pierce, R. B., Chatfield, R. B.,  
911 Oltmans, S. J., Cooper, O. R., Loucks, A. L., Taubman, B. F., Johnson, B. J., Joseph, E.,  
912 Kucsera, T. L., Merrill, J. T., Morris, G. A., Hersey, S., Forbes, G., Newchurch, M. J.,  
913 Schmidlin, F. J., Tarasick, D. W., Thouret, V., and Cammas, J.-P.: Intercontinental Chemical  
914 Transport Experiment Ozonesonde Network Study (IONS) 2004: 1. Summertime upper  
915 troposphere/lower stratosphere ozone over northeastern North America, *J. Geophys. Res.*, 112,  
916 doi: 10.1029/2006jd007441, 2007b.

917 Thompson, A. M., Witte, J. C., Smit, H. G. J., Oltmans, S. J., Johnson, B. J., Kirchhoff, V. W. J.  
918 H., and Schmidlin, F. J.: Southern Hemisphere Additional Ozonesondes (SHADOZ) 1998–2004  
919 tropical ozone climatology: 3. Instrumentation, station-to-station variability, and evaluation with  
920 simulated flight profiles, *J. Geophys. Res.*, 112, doi: 10.1029/2005jd007042, 2007c.

921 Thompson, A. M., Yorks, J. E., Miller, S. K., Witte, J. C., Dougherty, K. M., Morris, G. A.,  
922 Baumgardner, D., Ladino, L., and Rappenglück, B.: Tropospheric ozone sources and wave  
923 activity over Mexico City and Houston during MILAGRO/Intercontinental Transport



924 Experiment (INTEX-B) Ozonesonde Network Study, 2006 (IONS-06), *Atmos. Chem. Phys.*, 8,  
925 5113-5125, 2008.

926 Toon, O. B., Maring, H., Dibb, J., Ferrare, R., Jacob, D. J., Jensen, E. J., Luo, Z. J., Mace, G. G.,  
927 Pan, L. L., Pfister, L., Rosenlof, K. H., Redemann, J., Reid, J. S., Singh, H. B., Thompson, A.  
928 M., Yokelson, R., Minnis, P., Chen, G., Jucks, K. W., and Pszenny, A.: Planning,  
929 implementation, and scientific goals of the Studies of Emissions and Atmospheric Composition,  
930 Clouds and Climate Coupling by Regional Surveys (SEAC4RS) field mission, *J. Geophys. Res.*,  
931 121, 4967-5009, doi: 10.1002/2015jd024297, 2016.

932 van Oss, R. F., Voors, R. H. M., and Spurr, R. J. D.: Ozone profile algorithm, in: *OMI Algorithm*  
933 *Theoretical Basis Document, Volume II: OMI ozone products*, edited by: Bhartia, P. K.,  
934 Greenbelt, MD, 51-73, 2001.

935 Vasilkov, A., Joiner, J., Spurr, R., Bhartia, P. K., Levelt, P., and Stephens, G.: Evaluation of the  
936 OMI cloud pressures derived from rotational Raman scattering by comparisons with other  
937 satellite data and radiative transfer simulations, *J. Geophys. Res.-Atmos.*, 113, n/a-n/a, doi:  
938 10.1029/2007JD008689, 2008.

939 Veefkind, J. P., de Haan, J. F., Brinksma, E. J., Kroon, M., and Levelt, P. F.: Total Ozone From  
940 the Ozone Monitoring Instrument (OMI) Using the DOAS Technique, *IEEE T. Geosci. Remote.*,  
941 44, 1239-1244, 2006.

942 Wang, L., Newchurch, M. J., Biazar, A., Liu, X., Kuang, S., Khan, M., and Chance, K.:  
943 Evaluating AURA/OMI ozone profiles using ozonesonde data and EPA surface measurements  
944 for August 2006, *Atmos. Environ.*, 45, 5523-5530, doi: 10.1016/j.atmosenv.2011.06.012, 2011.

945 WMO: SPARC/IO3C/GAW Assessment of trends in the vertical distribution of ozone,  
946 GenevaRep. 43, 1998.

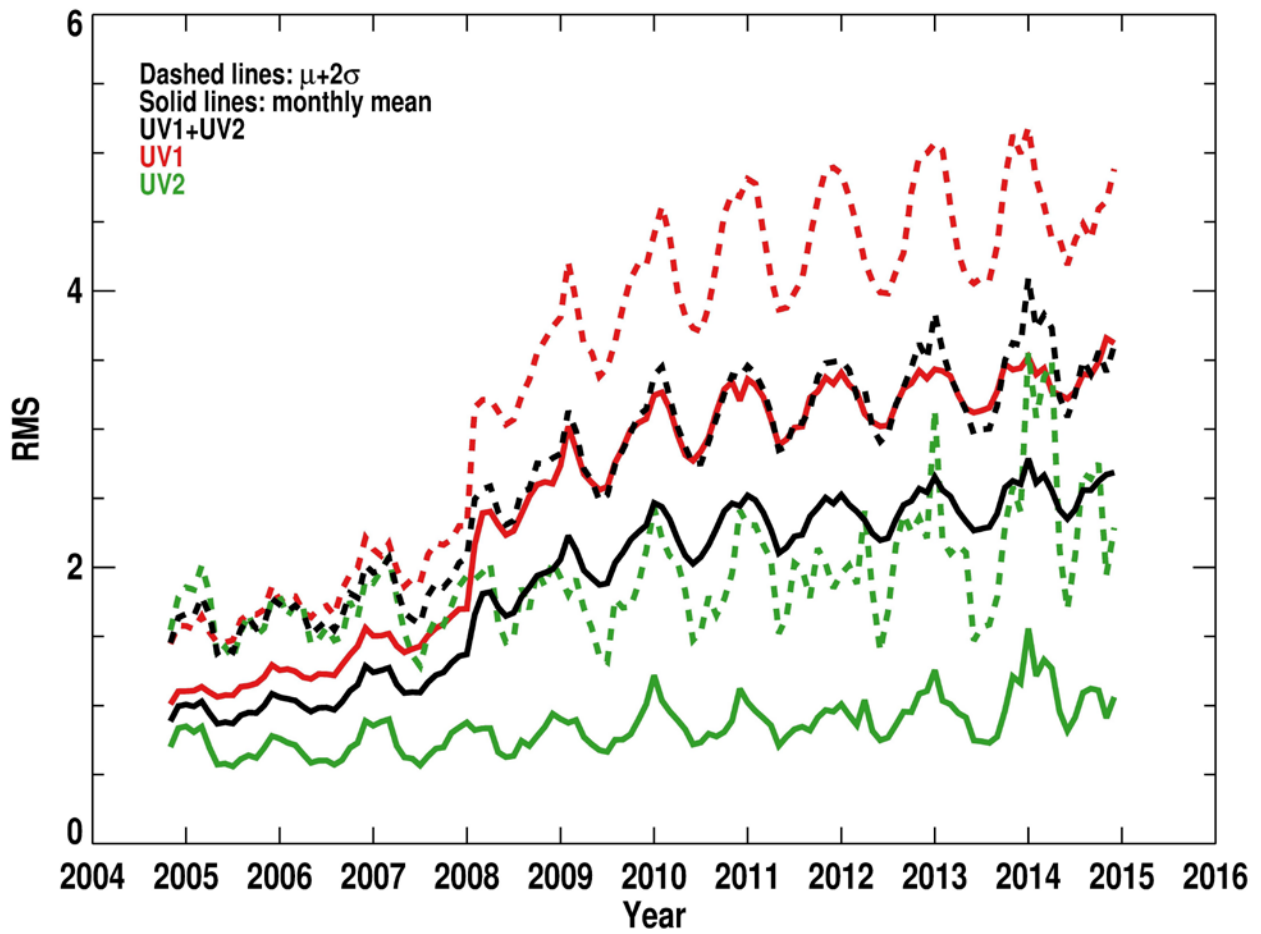
947 Worden, H. M., Logan, J. A., Worden, J. R., Beer, R., Bowman, K., Clough, S. A., Eldering, A.,  
948 Fisher, B. M., Gunson, M. R., Herman, R. L., Kulawik, S. S., Lampel, M. C., Luo, M.,  
949 Megretskaia, I. A., Osterman, G. B., and Shephard, M. W.: Comparisons of Tropospheric  
950 Emission Spectrometer (TES) ozone profiles to ozonesondes: Methods and initial results, *J.*  
951 *Geophys. Res.*, 112, doi: 10.1029/2006jd007258, 2007.

952 Yang, Q., Cunnold, D. M., Wang, H. J., Froidevaux, L., Claude, H., Merrill, J., Newchurch, M.,  
953 and Oltmans, S. J.: Midlatitude tropospheric ozone columns derived from the Aura Ozone  
954 Monitoring Instrument and Microwave Limb Sounder measurements, *J. Geophys. Res.: Atmos.*,  
955 112, D20305, doi: doi: 10.1029/2007JD008528, 2007.

956 Ziemke, J. R., Olsen, M. A., Witte, J. C., Douglass, A. R., Strahan, S. E., Wargan, K., Liu, X.,  
957 Schoeberl, M. R., Yang, K., Kaplan, T. B., Pawson, S., Duncan, B. N., Newman, P. A., Bhartia,  
958 P. K., and Heney, M. K.: Assessment and applications of NASA ozone data products derived  
959 from Aura OMI/MLS satellite measurements in context of the GMI chemical transport model, *J.*  
960 *Geophys. Res.*, 119, 5671-5699, doi: 10.1002/2013jd020914, 2014.

961

962

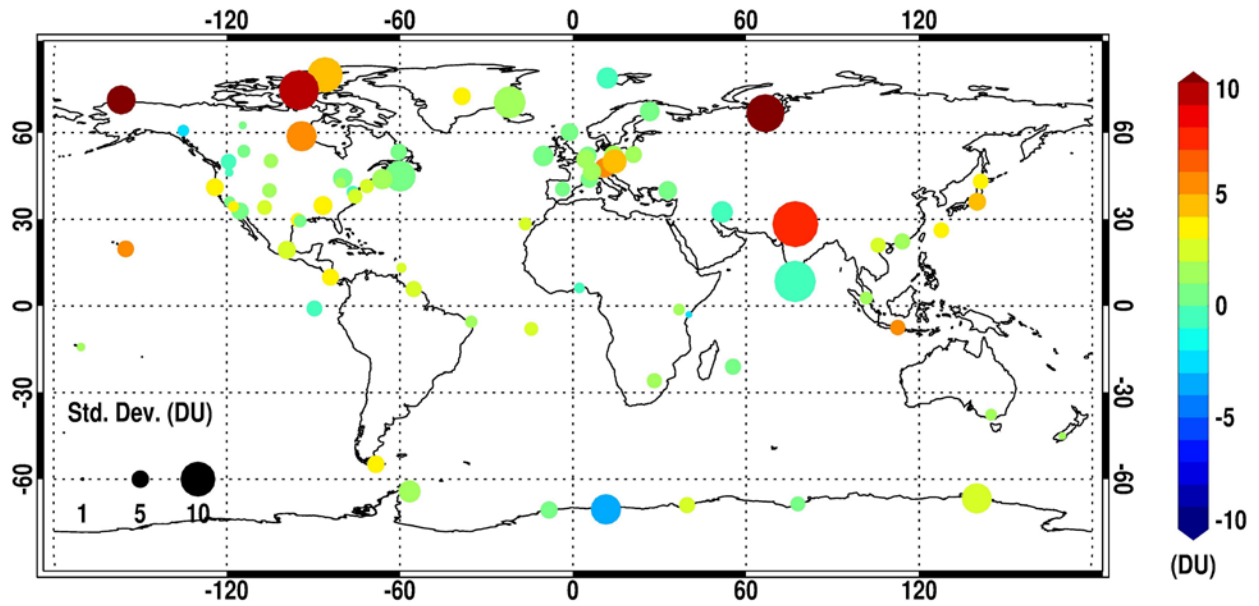


965

966 **Figure 1** Variation of monthly mean OMI RMS (defined as Root Mean Square of the ratio of  
967 radiance residuals to assumed radiance errors). The dashed and solid lines represent respectively  
968 the monthly mean RMS, and the sum of monthly mean plus its two standard deviations that is set  
969 as the RMS threshold for data screening.

970

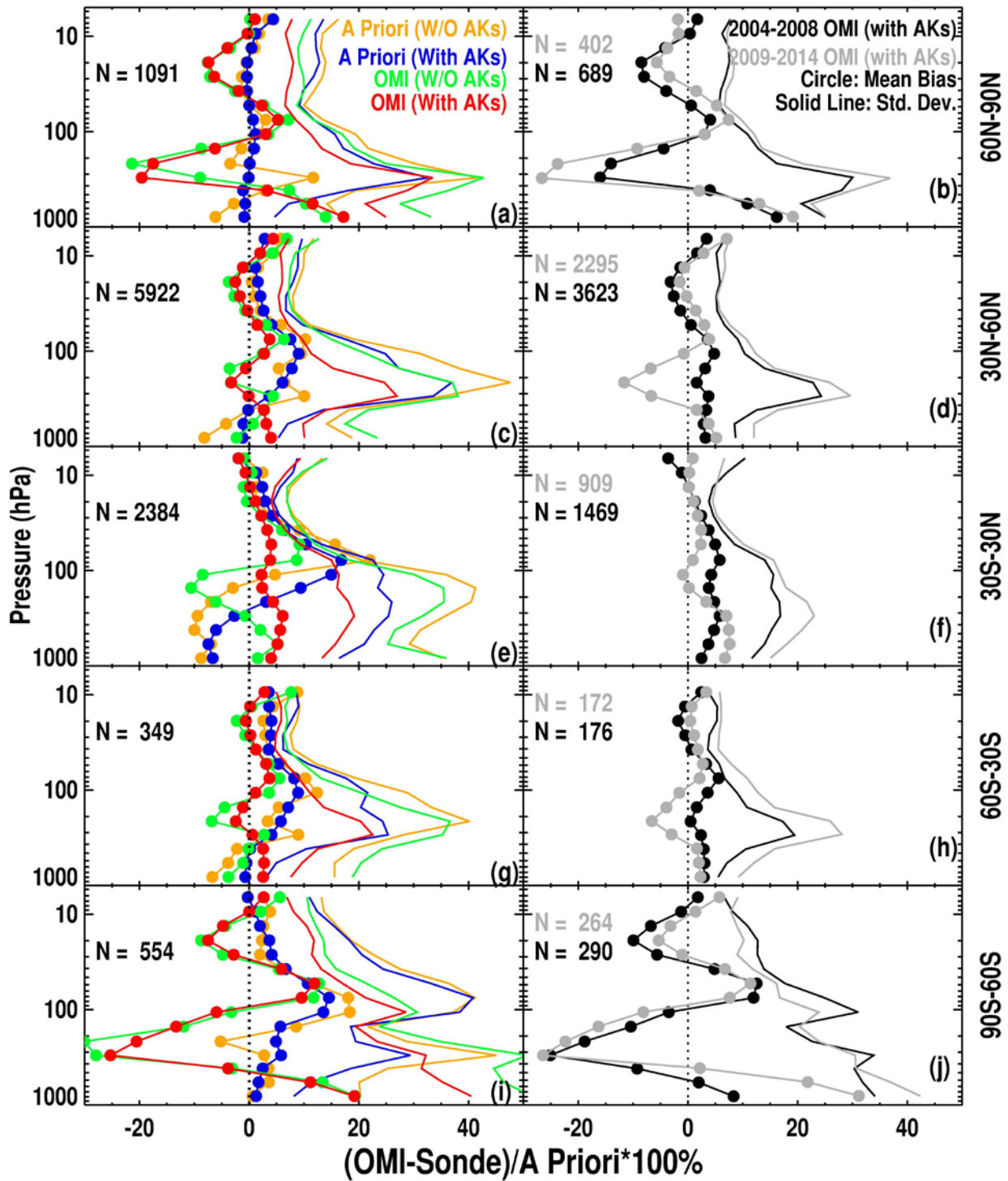
971



972

973 **Figure 2** The distribution of ozonesonde stations in this study. The color represents the mean biases  
974 between OMI and ozonesonde tropospheric ozone columns (TOCs) at each station (if the number of  
975 OMI and ozonesonde pairs is more than 10), and the dot size represents the standard deviation.

976



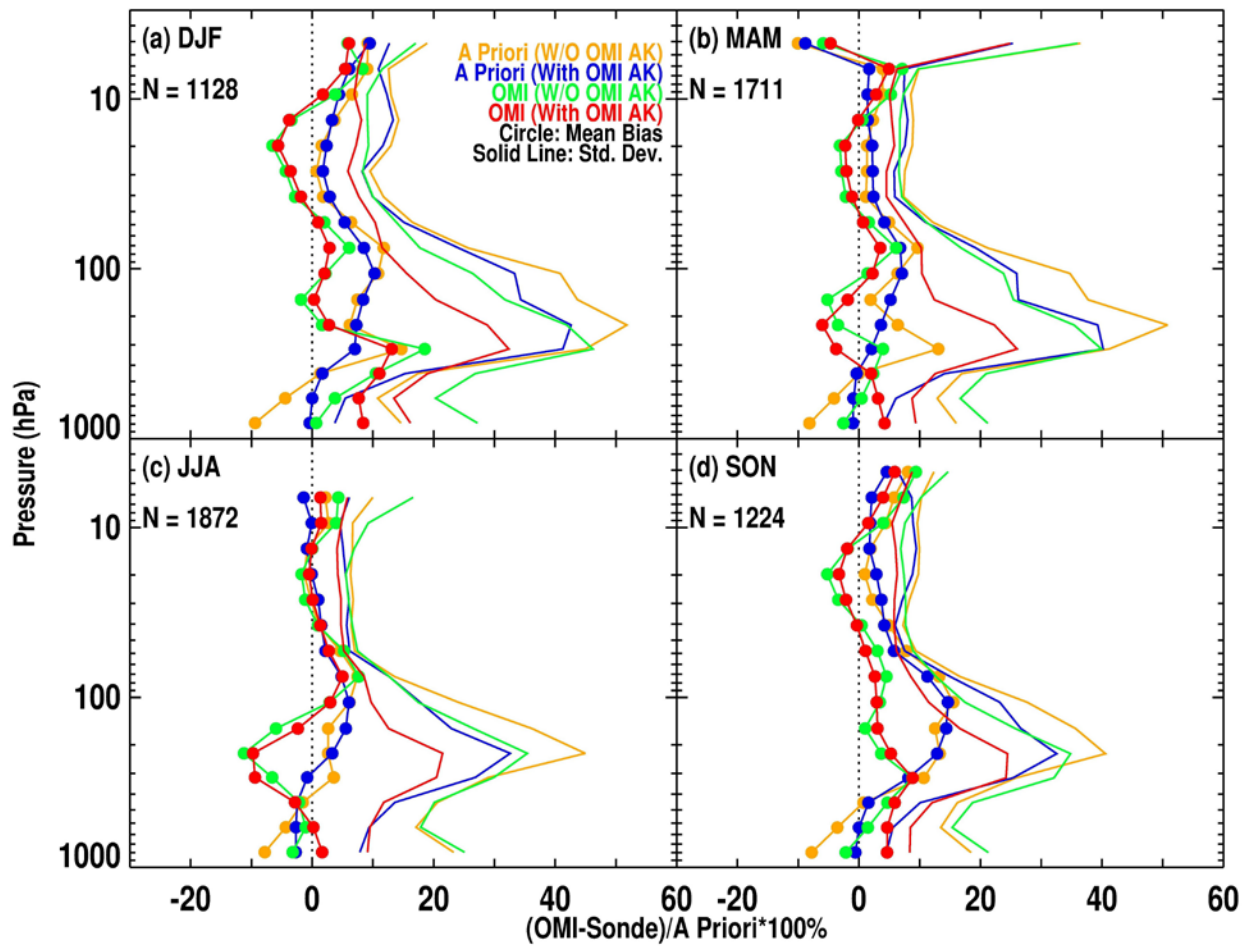
979 Figure 3 Mean relative biases in ozone (line with circles) and corresponding standard deviations  
 980 (solid lines) between OMI retrieval/a priori and ozonesondes with and without applying OMI  
 981 retrieval averaging kernels (i.e., with AKs, and W/O AKs in red and green for comparing retrievals

982 and in blue and yellow for comparing a priori) for five different latitude bands. The left panels  
983 show the comparison using 10 years of OMI data (2004-2014), and the right panels show the  
984 comparison between OMI retrieval and ozonesonde with OMI AKs for before and after the  
985 occurrence of serious OMI row anomaly (RA), i.e., pre-RA (2004-2008) in black and post-RA  
986 (2009-2014) in gray, respectively. The number (N) of OMI/ozonesonde coincidences used in the  
987 comparison is indicated in the legends.

988

989

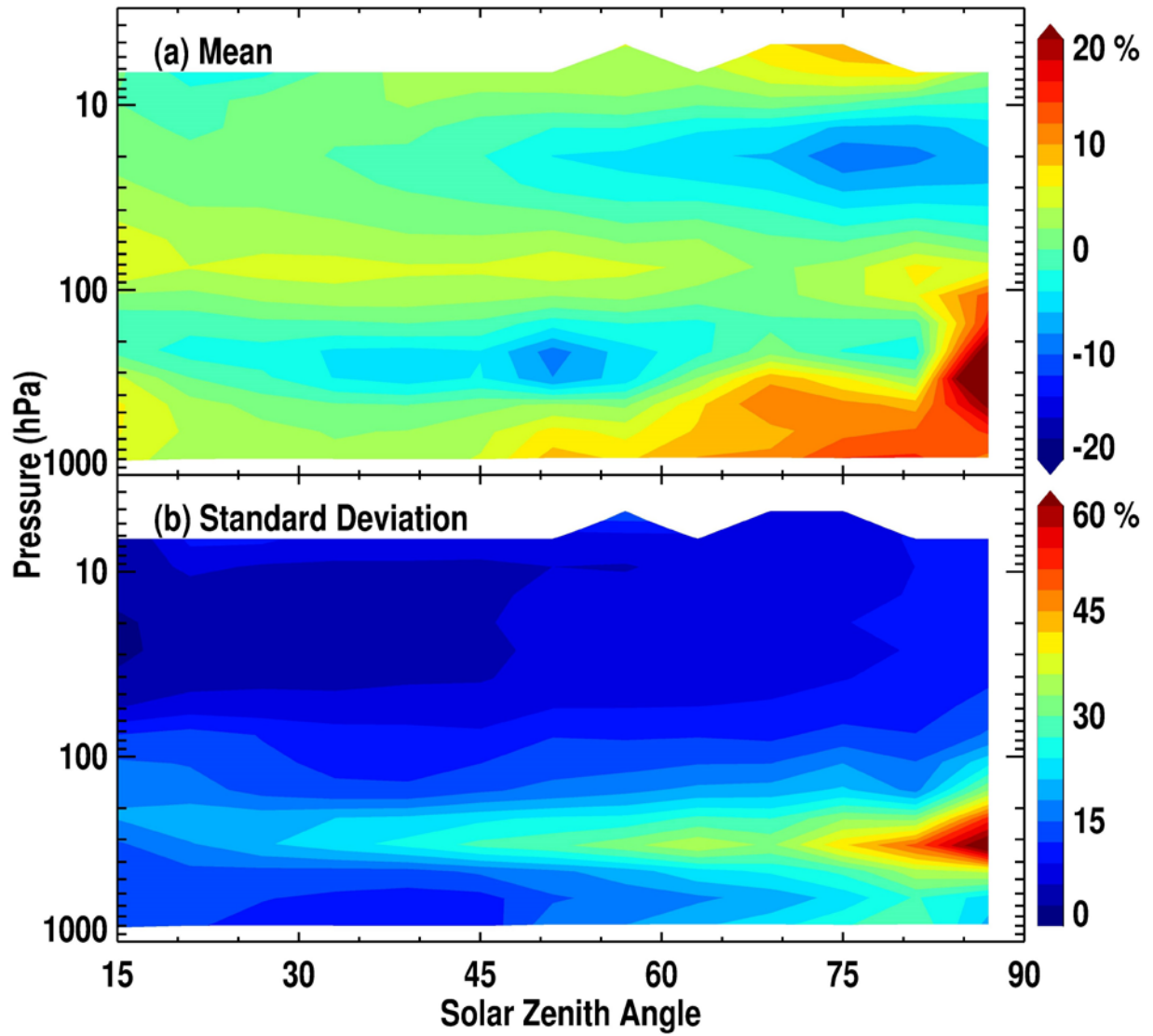
990



991

992 Figure 4 Same as Figure 3c but for each individual season at 30° N-60° N.

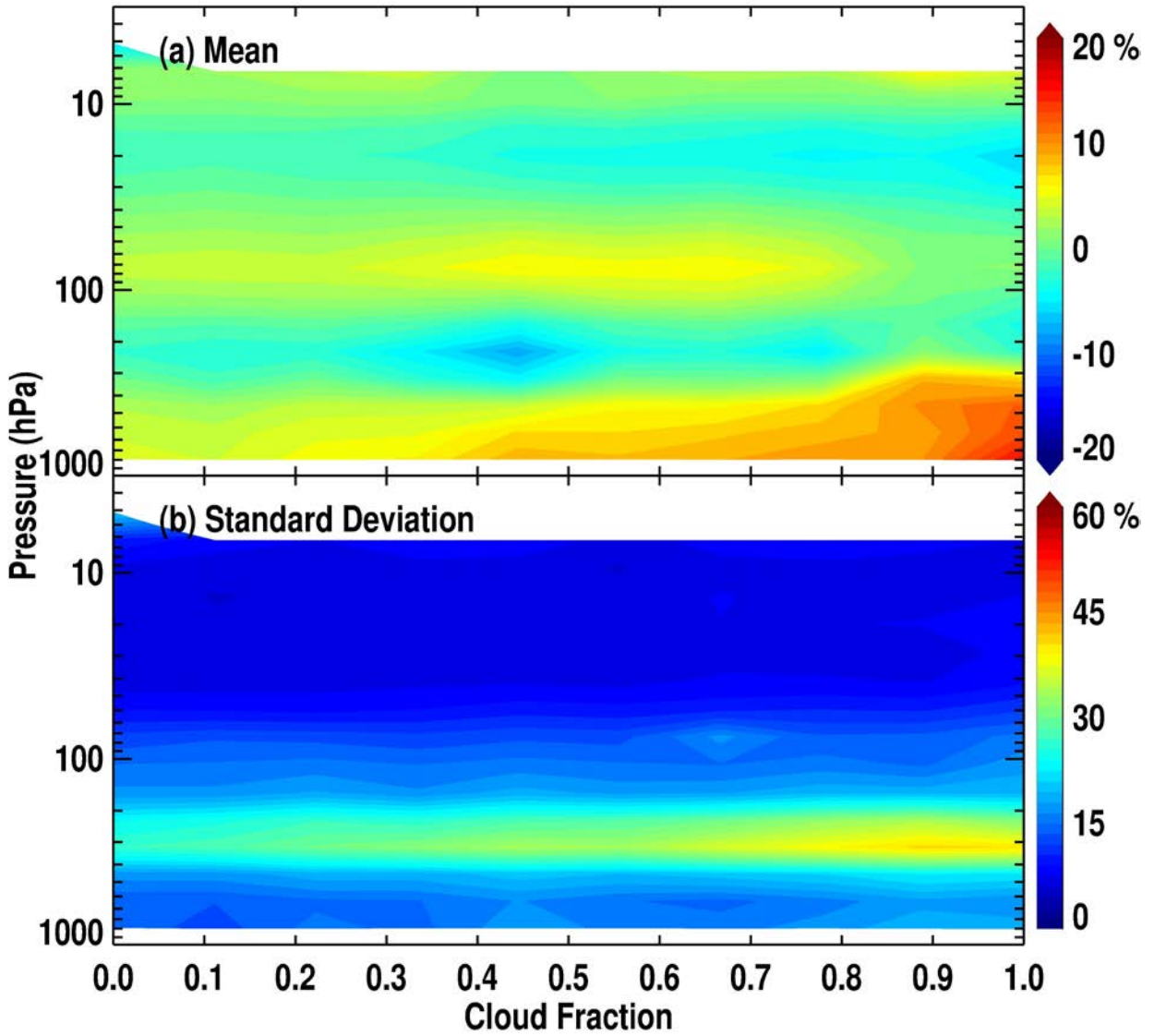
993



994

995 **Figure 5 Mean relative biases in ozone (a) and standard deviations (b) of the differences between**  
 996 **OMI and ozonesonde convolved with OMI AKs as a function of Solar Zenith Angle using all**  
 997 **OMI/ozonesonde coincidences during 2004-2014.**

998



1000

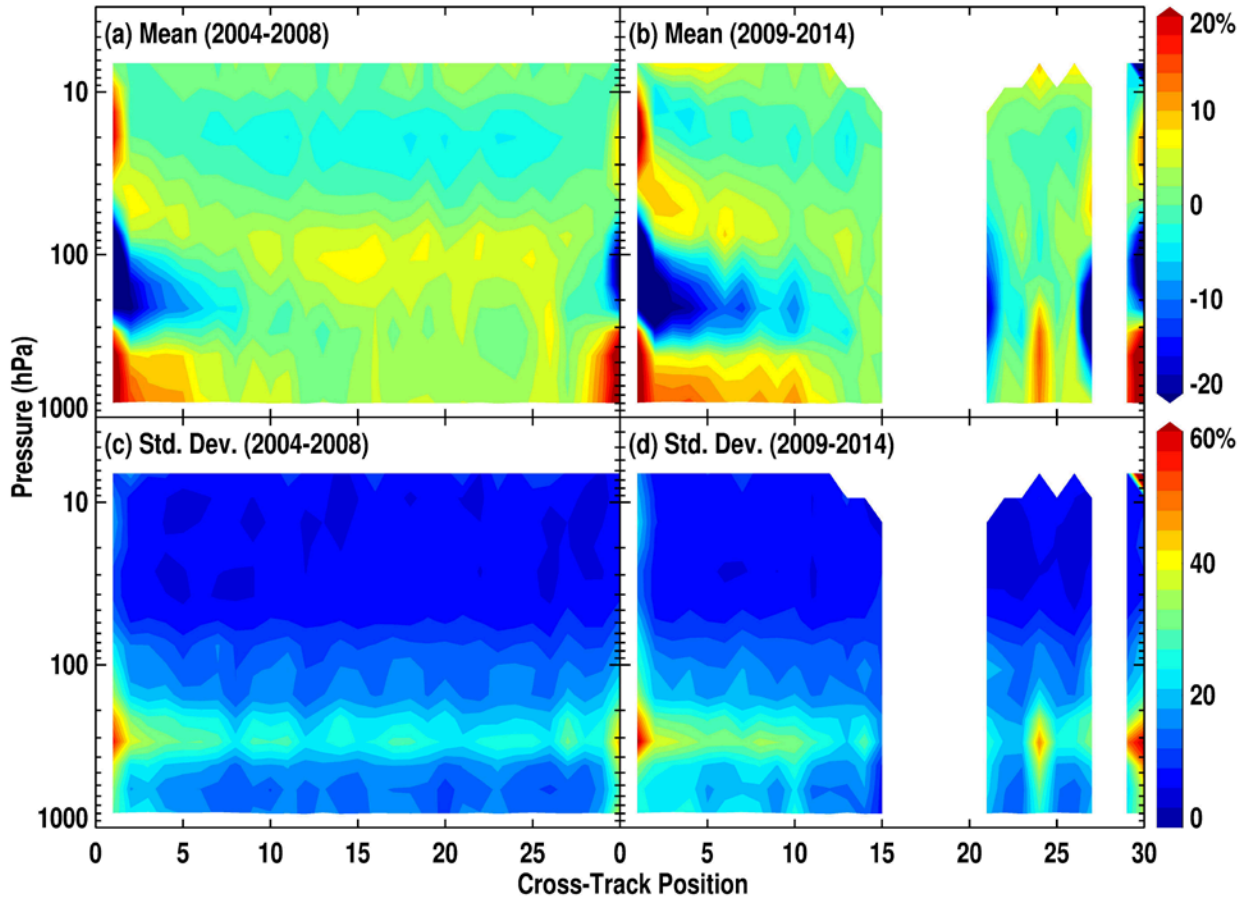
1001 **Figure 6** Same as **Figure 5** but as a function of cloud fraction.

1002



1003

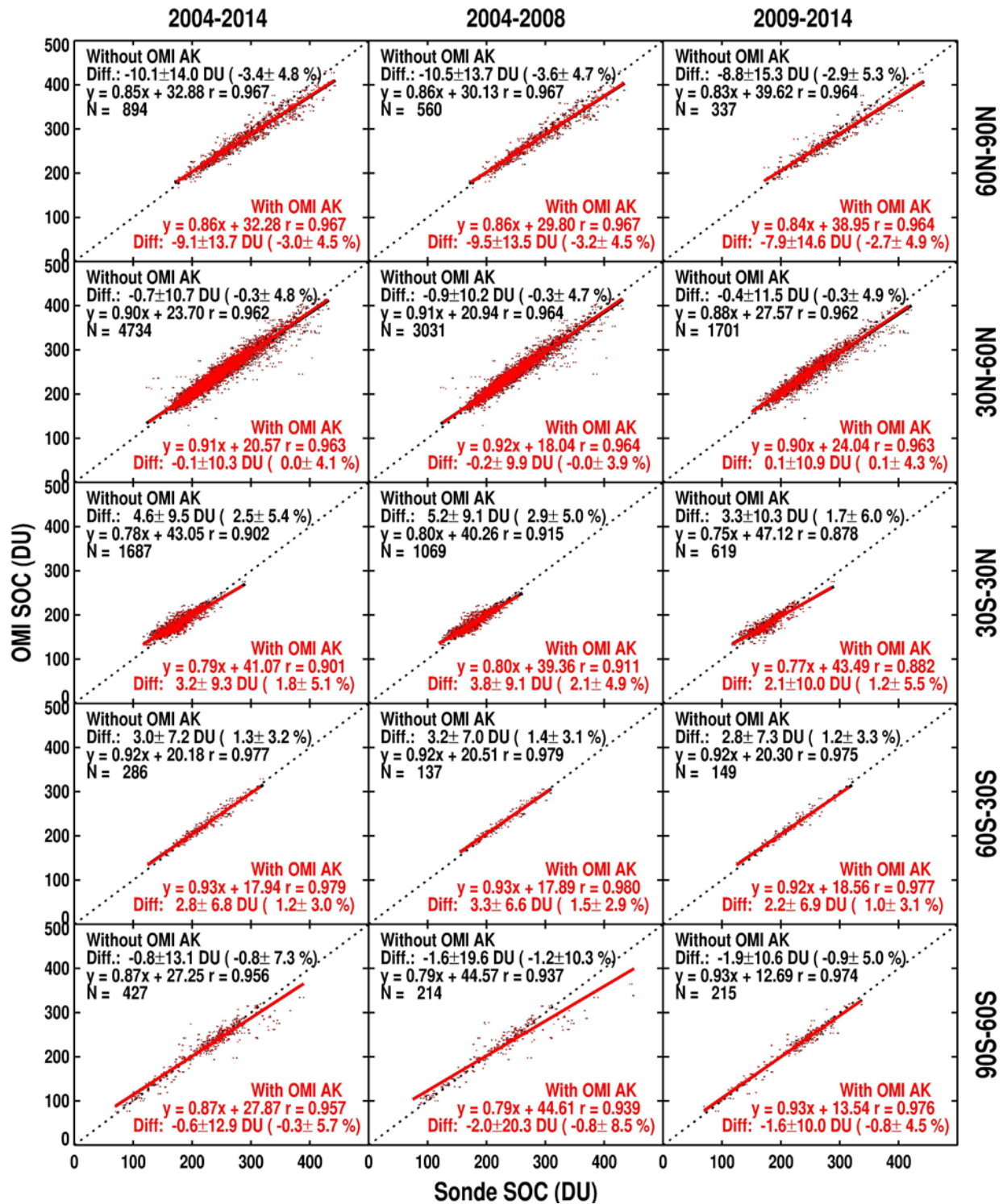
1004



1005

1006 **Figure 7** Same as **Figure 5** but as a function of cross-track position for (left) pre-RA (2004-2008)  
1007 and (right) post-RA (2009-2014) periods, respectively.

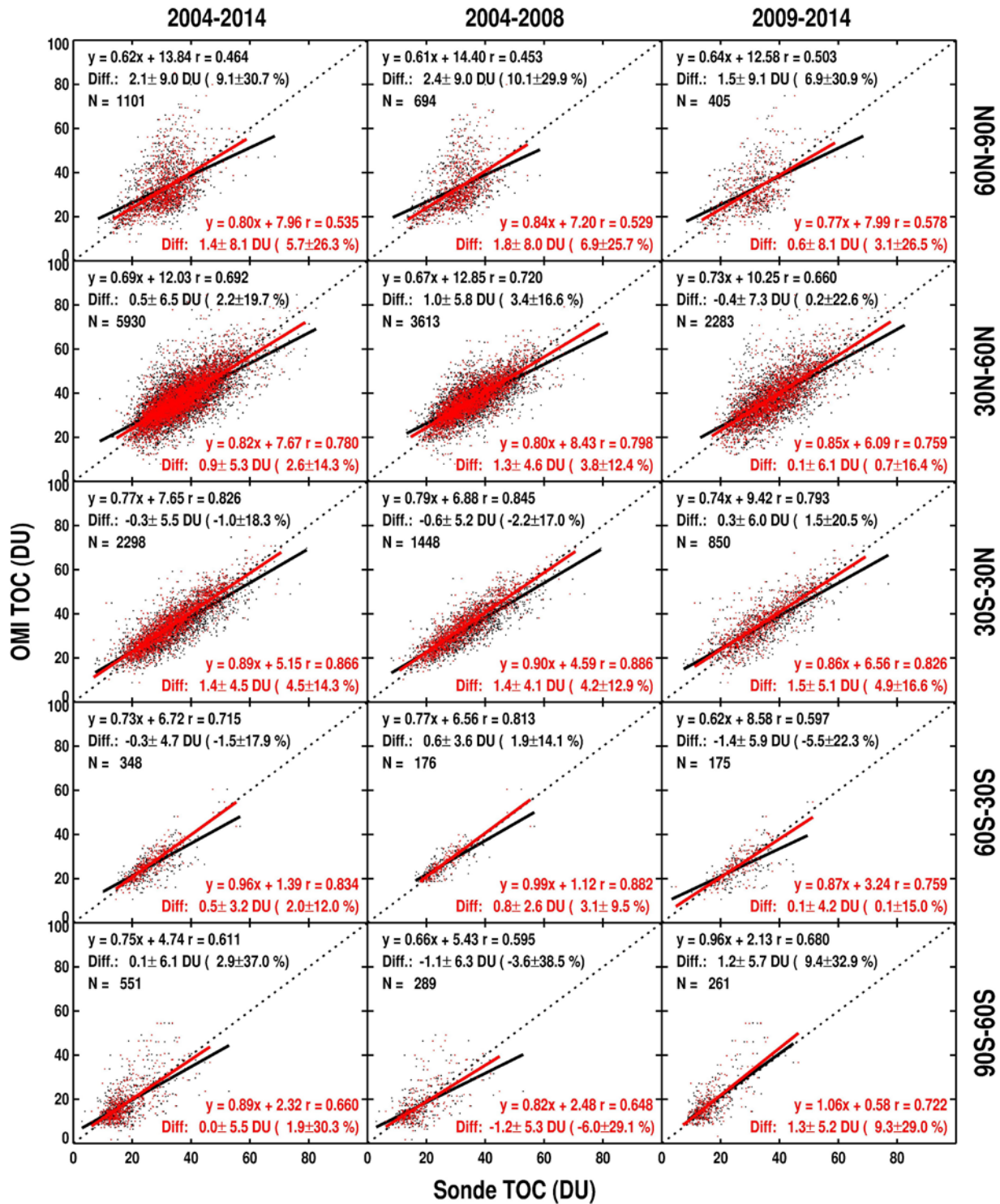
1008



1009

1010 Figure 8. Scattering plots of OMI Stratospheric Ozone Columns (SOCs) vs. ozonesonde SOC (DU) without (black) and with (red) average kernels for five different latitude bands during 2004-2014  
 1011 (left), the pre-row anomaly (RA) period (i.e., 2004-2008, middle) and the post-RA period (i.e., 2009-  
 1012 2014, right), respectively. Comparison statistics including mean biases and standard deviations in  
 1013

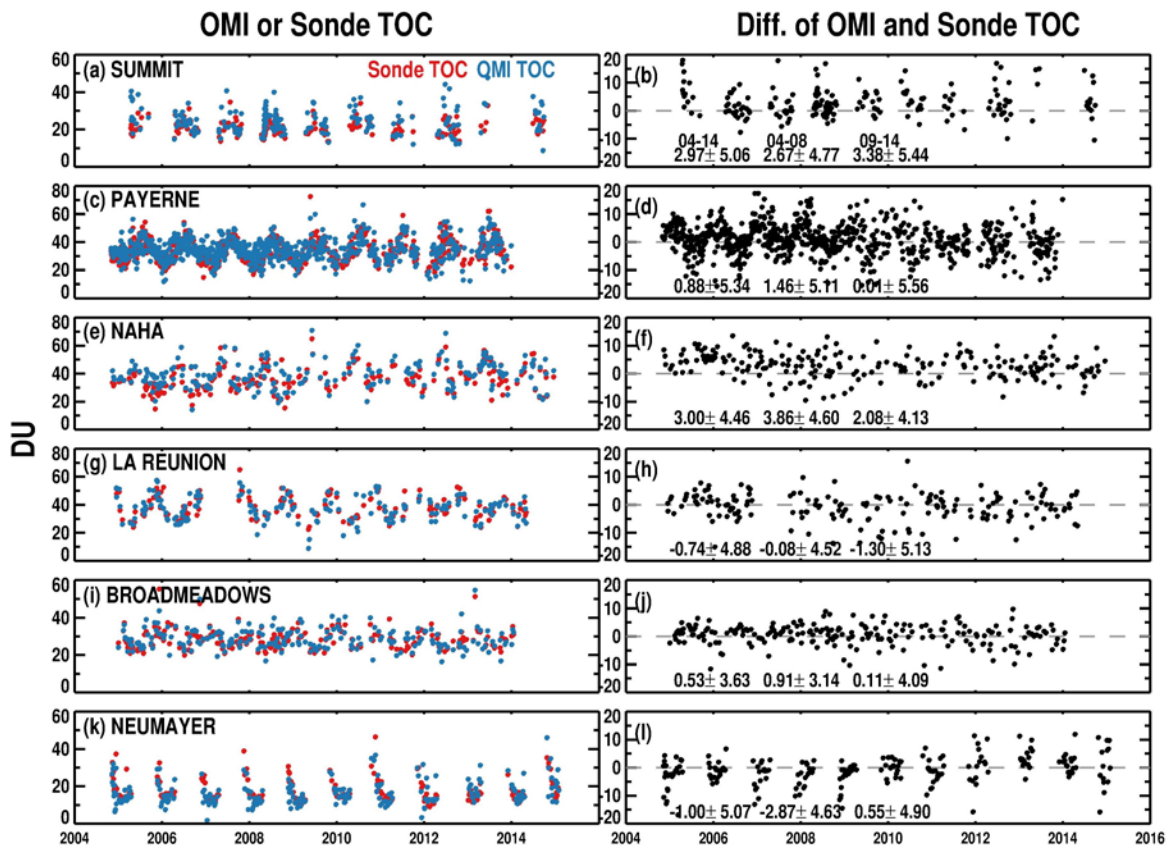
1014 **both DU and %, the linear regression and correlation coefficients in DU, and the number of**  
1015 **coincidences are shown in the legends.**



1017

1018 Figure 9. Similar to Figure 8, but for comparison of Tropospheric Ozone Columns (TOCs).

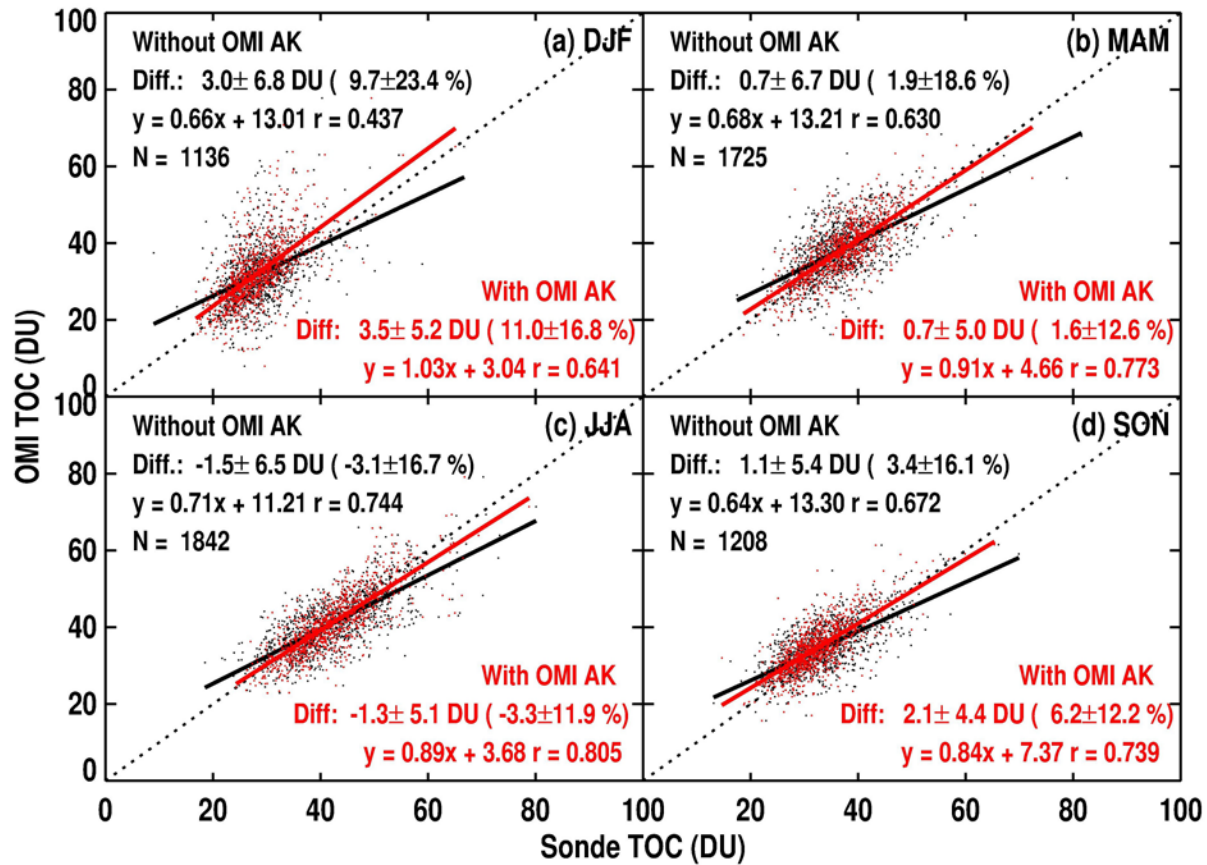
1019



1020

1021 **Figure 10. (Left) Time series of OMI tropospheric ozone columns (TOCs) as green dots and**  
 1022 **ozonesonde TOCs (with OMI AKs applied) in Summit (38.48° W, 72.57° N), Payene (6.57° E, 46.49°**  
 1023 **N), Naha (127.69° E, 26.21° N), La Réunion (55.48° E, 21.06° S), Broadmeadows (144.95° E, 58.74°**  
 1024 **S) and Neumayer (8.27° W, 70.68° S), and (Right) their corresponding differences, including the**  
 1025 **mean biases and standard deviations in 2004-2014, pre-RA (2004-2008) and post-RA (2009-2014)**  
 1026 **periods, respectively, in the legends.**

1027

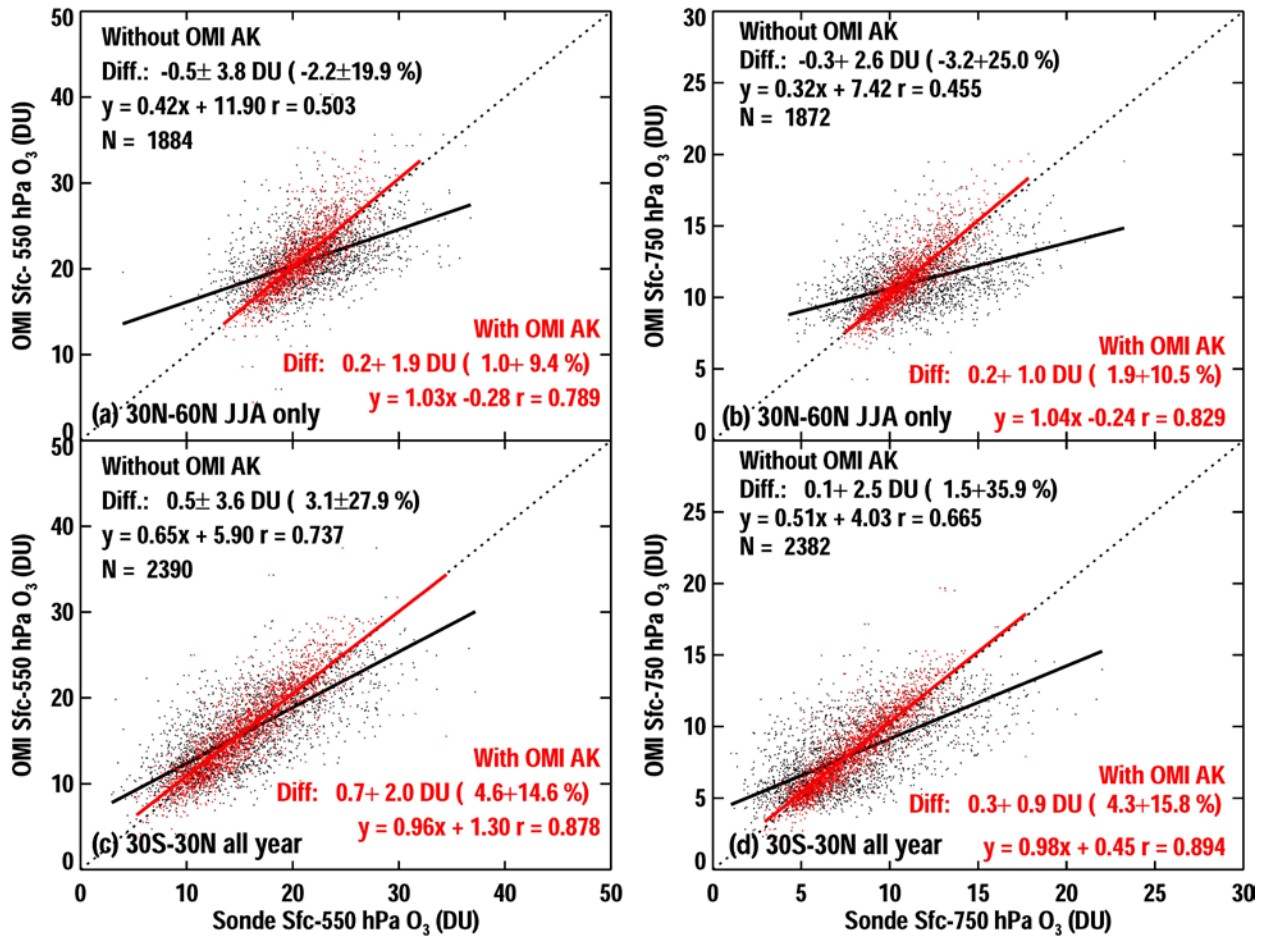


1028

1029 **Figure 11. Similar to Fig. 9 but for different seasons at northern middle latitude during the 2004-**  
 1030 **2014 period.**

1031

1032

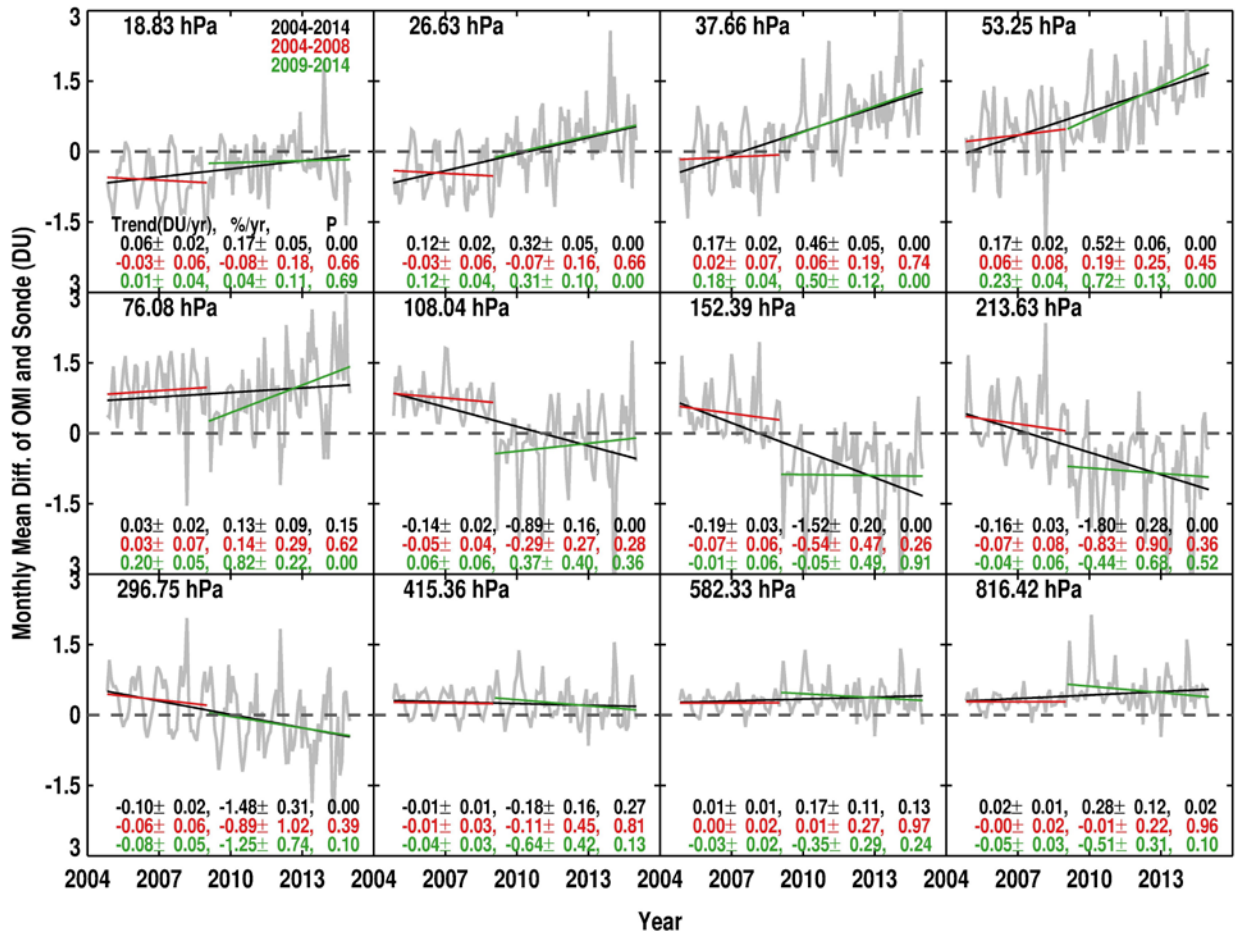


1033

1034 Figure 12. Similar to Fig. 9 but for comparison of lower tropospheric ozone columns during the  
1035 2004-2014 period. (a) Surface~550 hPa ozone column and (b) Surface~750 hPa ozone column in 30°  
1036 N-60° N during the summer, (c) and (d) same as (a) and (b) but for the tropics.

1037

1038



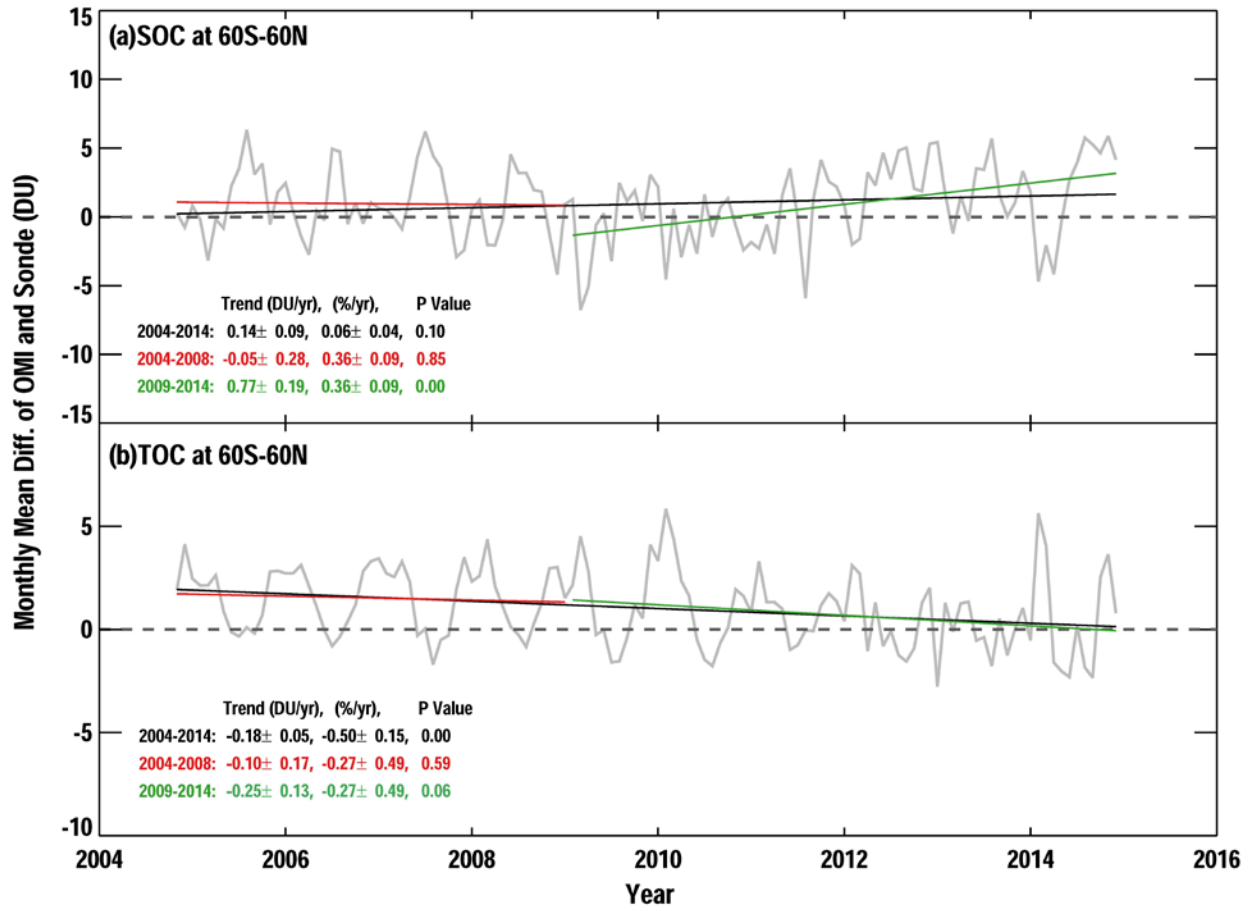
1039

1040 **Figure 13. Monthly mean variation of OMI and ozonesonde mean biases in 60° N-60° S at each**  
 1041 **OMI layer. OMI retrieval averaging kernels are applied to ozonesonde data. The black, red and**  
 1042 **green lines represent the linear ozone bias trends in 2004-2014, pre-RA (2004-2008) and post-RA**  
 1043 **(2009-2014), respectively. The average altitude of each layer is marked on the left corner of each**  
 1044 **grid. The trends in DU/yr or % yr and P value for each time period are indicated in the legends.**

1045



1046



1047

1048 Figure 14. Same as Figure 13 but for Stratospheric Ozone Columns (SOCs) and Tropospheric  
1049 Ozone Columns (TOCs).